AD-A136 722 THIN FILM TECHNOLOGY OF HIGH-CRITICAL-TEMPERATURE SUPERCONDUCTING ELECTRO.. (U) WESTINGHOUSE RESEARCH AND DEVELOPMENT CENTER PITTSBURGH PA J TALVACCHIO ET AL. 1/1

UNCLASSIFIED 05 DEC 83 83-9C9-TUDEV-R1 F/G 20/12 NL

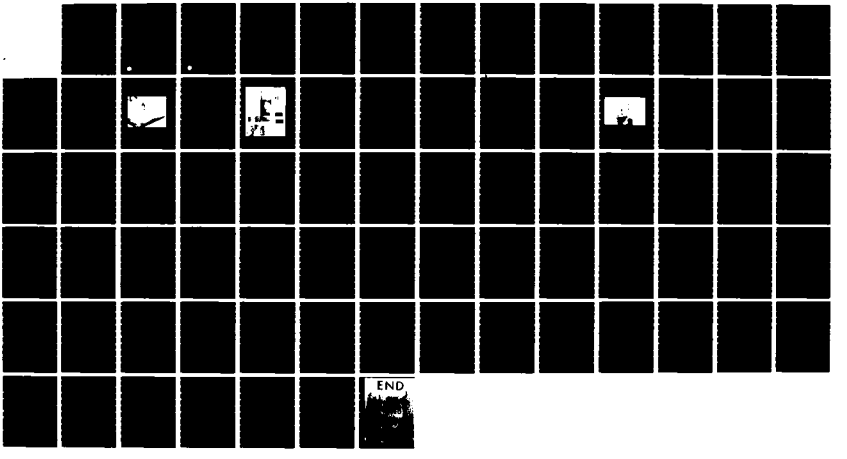

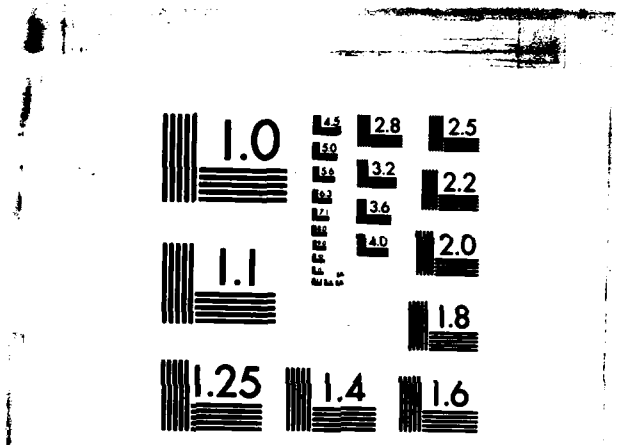

MICROCOPY RESOLUTION TEST CHART
NATIONAL BUREAU OF STANDARDS-1963-A

THIN FILM TECHNOLOGY OF HIGH-CRITICAL-TEMPERATURE SUPERCONDUCTING ELECTRONICS

(12)

A136722

Annual Report

Covering the Period

August 1, 1982 to October 30, 1983

J. Talvacchio, A. I. Braginski, J. R. Gavaler,

M. A. Janocko, A. S. Manocha, and R. D. Blaugher

Prepared for

the Office of Naval Research

Under Contract No. N00014-82-C-0617

by

Westinghouse Electric Corporation

Research and Development Center

Pittsburgh, Pennsylvania 15235

December 5, 1983

Westinghouse R&D Center
1310 Beulah Road
Pittsburgh, Pennsylvania 15235

THIN FILM TECHNOLOGY OF HIGH-CRITICAL-TEMPERATURE SUPERCONDUCTING ELECTRONICS

Annual Report

Covering the Period

August 1, 1982 to October 30, 1983

J. Talvacchio, A. I. Braginski, J. R. Gavaler,

M. A. Janocko, A. S. Manocha, and R. D. Blaugher

Prepared for

the Office of Naval Research

Under Contract No. N00014-82-C-0617

by

Westinghouse Electric Corporation

Research and Development Center

Pittsburgh, Pennsylvania 15235

December 5, 1983

Westinghouse R&D Center
1310 Beulah Road
Pittsburgh, Pennsylvania 15235

Unclassified
SECURITY CLASSIFICATION OF THIS PAGE

AD-A136 722

REPORT DOCUMENTATION PAGE

1a. REPORT SECURITY CLASSIFICATION	1b. RESTRICTIVE MARKINGS
2a. SECURITY CLASSIFICATION AUTHORITY	3. DISTRIBUTION/AVAILABILITY OF REPORT
2b. DECLASSIFICATION/DOWNGRADING SCHEDULE	
4. PERFORMING ORGANIZATION REPORT NUMBER(S) 83-9C9-TUDEV-R1	5. MONITORING ORGANIZATION REPORT NUMBER(S)
6a. NAME OF PERFORMING ORGANIZATION Westinghouse Research and Development Center 6b. OFFICE SYMBOL (If applicable)	7a. NAME OF MONITORING ORGANIZATION DCASMA Pittsburgh
6c. ADDRESS (City, State and ZIP Code) 1310 Beulah Road Pittsburgh, Pennsylvania 15235	7b. ADDRESS (City, State and ZIP Code) 1626-S Federal Building 1000 Liberty Avenue Pittsburgh, Pennsylvania 15222
8a. NAME OF FUNDING/SPONSORING ORGANIZATION Office of Naval Research 8b. OFFICE SYMBOL (If applicable)	9. PROCUREMENT INSTRUMENT IDENTIFICATION NUMBER
8c. ADDRESS (City, State and ZIP Code) 800 North Quincy Street Arlington, Virginia 22217	10. SOURCE OF FUNDING NOS. PROGRAM ELEMENT NO. / PROJECT NO. / TASK NO. / WORK UNIT NO.
11. TITLE (Include Security Classification) THIN FILM TECHNOLOGY OF HIGH-CRITICAL-TEMPERATURE SUPERCONDUCTING ELECTRONICS	
12. PERSONAL AUTHOR(S) Talvacchio, J; Braginski, A.I.; Gavaler, J.R.; Janocko, M.A.,: Manocha, A.S.; Baugher, R.D	
13a. TYPE OF REPORT Annual 13b. TIME COVERED FROM 8-1-82 TO 10-30-83	14. DATE OF REPORT (Yr., Mo., Day) 831205 15. PAGE COUNT 65
16. SUPPLEMENTARY NOTATION	
17. COSATI CODES FIELD / GROUP / SUB. GR.	18. SUBJECT TERMS (Continue on reverse if necessary and identify by block number) superconductors, films, sputtering, Josephson, junctions, niobium, vanadium, molybdenum, A15, oxidation, XPS.

19. ABSTRACT (Continue on reverse if necessary and identify by block number)

The objective of the first year's work was to investigate A15 superconductor/barrier oxide interfaces, identify oxide depth profiles, and determine resulting tunneling characteristics using soft tunnel junction counterelectrodes. Bilayers consisting of Nb and vanadium-silicon (A15) base electrodes and thin Y, Al, and Si barriers have been deposited in-situ and oxidized in humid air for up to three days. XPS analysis was used to compare the barrier coverage, uniformity, oxidation, and ability to protect the base electrode from oxidation for three deposition techniques: dc magnetron sputtering, dc diode sputtering, and reactive diode sputtering followed by pyrolysis. Y and Al have been found to be fully oxidized due to long oxidation times. In the above conditions the overlayers did not protect the superconductors from oxidation/hydration, and the surface of oxidized vanadium-silicon was also degraded by atomic segregation. The tunneling I-V characteristics exhibited very high leakage currents also suggestive of incomplete superconductor coverage by the metallic overlayer. Mo-Re was investigated

20. DISTRIBUTION/AVAILABILITY OF ABSTRACT UNCLASSIFIED/UNLIMITED ☐ SAME AS RPT. ☐ DTIC USERS ☐	21. ABSTRACT SECURITY CLASSIFICATION
22a. NAME OF RESPONSIBLE INDIVIDUAL	22b. TELEPHONE NUMBER (Include Area Code) / 22c. OFFICE SYMBOL

DD FORM 1473, 83 APR EDITION OF 1 JAN 73 IS OBSOLETE.

Unclassified
SECURITY CLASSIFICATION OF THIS PAGE

19. for its potential as a high-critical-temperature counterelectrode. A very low oxidation rate was found indicating potential compatibility with yttrium hydroxide-sealed barriers. Low temperature growth (60°C) of MoRe (86 at. % Mo) with only a 5% decline in critical temperature has been demonstrated. Work will continue in a closed system to eliminate the base superconductor degradation, reduce leakage and study high-critical-temperature counterelectrodes.

ANNUAL REPORT

AUGUST 1, 1982 TO OCTOBER 30, 1983

THIN FILM TECHNOLOGY OF HIGH-CRITICAL-TEMPERATURE SUPERCONDUCTING ELECTRONICS

by

J. Talvacchio, A.I. Braginski, J.R. Gavaler,
M.A. Janocko, A.S. Manocha and R.D. Blaugher

Westinghouse Electric Corporation
Research and Development Center
Pittsburgh, Pennsylvania 15235

ONR Contract No. N00014-82-C-0617

TABLE OF CONTENTS

ABSTRACT

The objective of the first year's work was to investigate A15 superconductor/barrier oxide interfaces, identify oxide depth profiles, and determine resulting tunneling characteristics using soft tunnel junction counterelectrodes. Bilayers consisting of Nb and V_3Si (A15) base electrodes and thin Y, Al, and Si barriers have been deposited *in situ* and oxidized in humid air for up to three days. XPS analysis was used to compare the barrier coverage, uniformity, oxidation, and ability to protect the base electrode from oxidation for three deposition techniques: dc magnetron sputtering, dc diode sputtering, and reactive diode sputtering followed by pyrolysis. Y and Al have been found to be fully oxidized due to long oxidation times. In the above conditions the overlayers did not protect the superconductors from oxidation/hydration, and the surface of oxidized V_3Si was also degraded by atomic segregation. The tunneling I-V characteristics exhibited very high leakage currents also suggestive of incomplete superconductor coverage by the metallic overlayer. Mo-Re was investigated for its potential as a high-T_c counterelectrode. A very low oxidation rate was found indicating potential compatibility with yttrium hydroxide-sealed barriers. Low temperature growth (60°C) of $Mo_{86}Re_{14}$ with only a 5% decline in T_c has been demonstrated. Work will continue in a closed system to eliminate the base superconductor degradation, reduce leakage and study high-T_c counterelectrodes.

LIST OF FIGURES

LIST OF TABLES

1. INTRODUCTION

1.1 Program Objective

The overall objective of this program is to develop a technology of thin-film Josephson junctions capable of operating at temperatures $T_{op} \geq 10K$, compatible with the performance of small closed-cycle refrigerators. This will permit the incorporation of superconducting electronics into electronic warfare and advanced radar systems.

The specific program objective (Phase I) is to demonstrate the technical feasibility of thin film tunnel junctions fabricated from A15 compounds and hard alloy superconductors, such as Mo-Re, having critical temperatures, T_c, sufficiently high to achieve useful device characteristics at temperatures exceeding T = 10K. This will permit the comparison with high-T_c, B-1 structure NbCN junctions developed by the Naval Research Laboratory and several other R&D organizations in the United States and overseas.

The first year's tasks defined by the Statement of Work are:

1. Investigate A15/rare-earth oxide and Mo-Re/oxide interfaces to identify the oxide species and their depth profiles.
2. Develop a selective anodization process for A15 films.
3. Fabricate tunnel junctions with artificial rare-earth oxide barriers and soft alloy or Nb-counterelectrodes (to be completed in the second year of performance).

1.2 Approach

The approach is based on the assumed use of a novel ultra-high-vacuum (UHV) thin film fabrication/analytical closed system. This will make possible the in-situ formation, processing and characterization (without breaking the vacuum) of multilayered, complete junction structures. These structures will be subsequently patterned into junctions by a selective anodization or etching process. A diagram of a multilayered structure is shown in Figure 1.1.

The key problems to be solved are:

1. To find an artificial tunneling barrier material (I in Figure 1.1)performing best with high-T_c junction electrodes, SC1 and SC2.
2. To form a counterelectrode (SC2) having a high-T_c within less than the coherence length, ξ_{GL}, from the barrier/counterelectrode interface (ξ_{GL} is of the order of 50 Å in high-T_c materials).

The first problem is being tackled through comparative X-ray photoelectron spectroscopy of superconductor/barrier bilayers. The oxidation and hydrolysis characteristics of a thin rare-earth (yttrium) layer on a superconducting base are compared with those of more conventional artificial barrier metals such as silicon and aluminum. A layer best protecting the base electrode from oxidation, and permitting the highest possible processing temperature without an excessive interdiffusion with electrodes is sought. The XPS results are correlated with tunneling characteristics obtained by forming junctions with lead or lead alloy counterelectrodes.

The second problem is to be approached through the search for a counterelectrode material having T_c insensitive to near-substrate crystalline disorder (Mo-Re ?) or capable of ordered polycrystalline epitaxial growth (A15 ?) on a "seeding" layer represented by the barrier itself or by a very thin normal metal proximity layer (N2 in Figure 1.1).

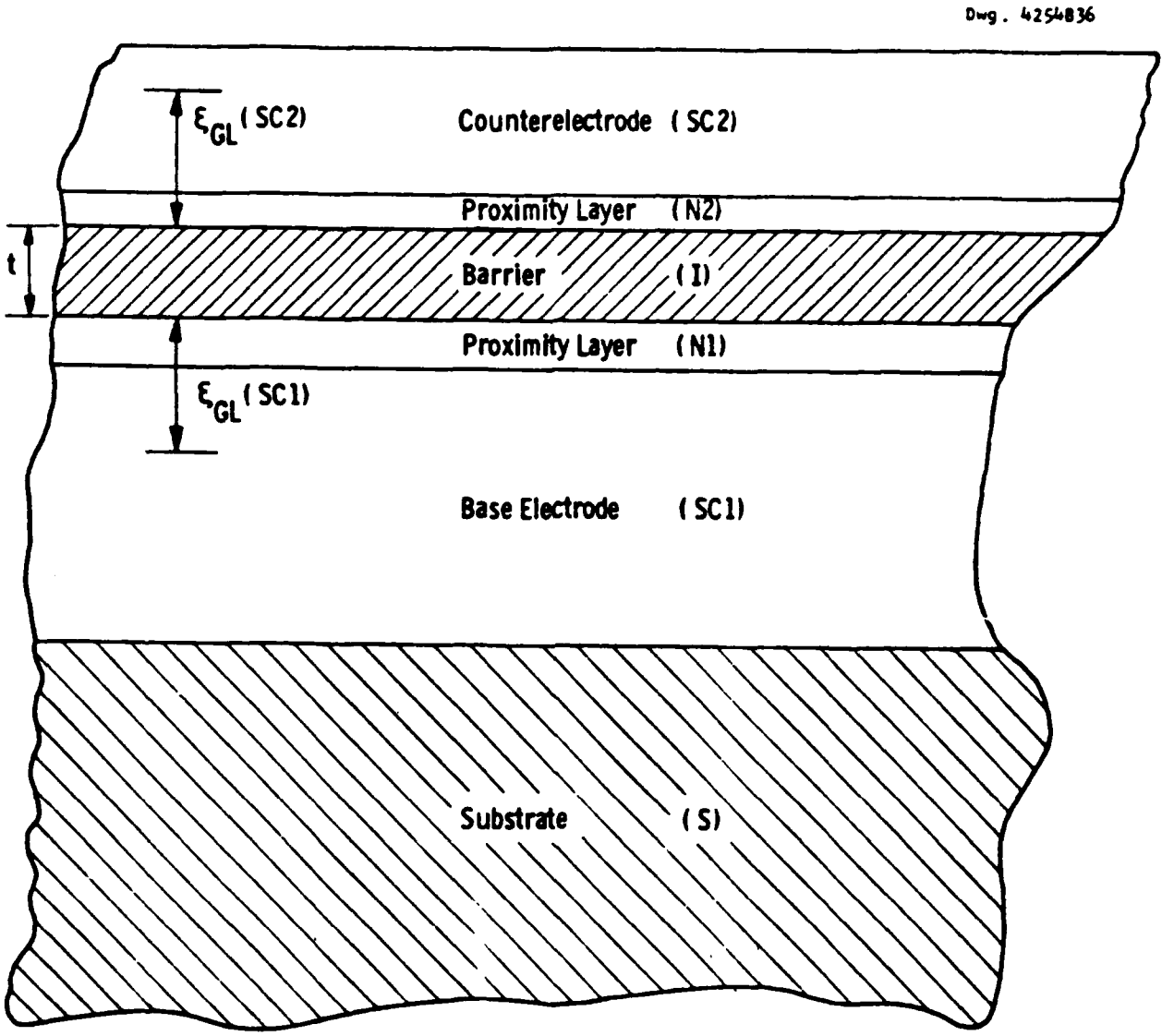

Figure 1.1 Tunnel junction layer structure.

1.3 Summary of Results

Thin films of Nb, V_3Si and Mo-Re have been fabricated by dc diode sputtering, reactive dc diode sputtering assisted by silane decomposition, and dc magnetron sputtering to obtain material properties suitable for high-T_{op} tunnel junctions. The Nb and V_3Si films were coated *in situ* with metallic overlayers of either Y, Al or Si up to 55 Å (78 Å) thick to form an oxide tunneling barrier upon exposure to air at room temperature. The surface oxidation of these bilayers was extensively studied by X-ray photoelectron spectroscopy (XPS). The oxide/hydroxide species and their thicknesses were thus determined. Long exposure times, up to 72 hours in humid air, resulted in a complete oxidation of metallic overlayers and the formation of underlying native oxides of Nb, V and Si (except for a single 78 Å thick Al overlayer on Nb). In V_3Si the oxidation also resulted in a significant Si-enrichment near the surface. Comparison with the literature data indicated that the high ambient humidity promoted the growth of oxides and of Y hydroxide. Thickest overlayers of Y on Nb, and Al on Nb and V_3Si, were found by XPS to grain-boundary diffuse into the superconductor at temperatures between 100°C and 250°C, in qualitative agreement with literature. These XPS data suggested that Y wets the V_3Si surface less well than Al. Tunnel junctions have been fabricated by evaporating lead counterelectrodes on the oxidized bilayers. Very high subgap leakage currents were tentatively attributed to the oxidation and degradation of base electrodes due to insufficient protection by fully oxidized overlayers, and, possibly, incomplete coverage. It is expected that thicker overlayers, and short oxidation times in a dry or controlled humidity atmosphere will result in low leakage, Pb-counterelectrode junctions. Once this is achieved work will concentrate on junctions patterned from *in situ* fabricated trilayers with a refractory (Nb) and high-T_c top layer.

2. EXPERIMENTAL APPARATUS AND METHODS

2.1 The DC Diode Sputter Apparatus

Starting at the end of September, 1982, and until May, 1983, superconducting films and superconductor/barrier bilayers had been fabricated in the dc diode sputtering system shown in Figure 2.1. The system existed prior to the inception of this program and was adapted for the *in situ* overlayer fabrication. The operating mode was as follows:

Eight 6 x 6 mm sapphire substrates were firmly clamped onto a massive molybdenum block (boat) for good thermal contact. A transfer mechanism permitted one to quickly transfer the block from position 1 (Figure 2.1)to position 2 without breaking the vacuum. In position 1 the block was radiant heated up to 1000°C and the superconducting film was dc sputtered from a Nb or V+Si elemental target. Temperature control was ensured by a Pt-PtRh thermocouple mounted in the movable boat. In position 2 the boat rested on a massive copper block that served as a heat sink and was capable of oscillation to ± 180°. In this position the Si barrier overlayer was dc sputtered at, nominally, room temperature after the deposition of the base electrode superconducting film. The target-substrate spacing was ∿1.9 cm (0.75 inch) in both positions. After the overlayer deposition the samples had been removed from the chamber so that the overlayer was oxidized in the ambient atmosphere.

The system had been operating with a low pumping speed oil diffusion pump and a mechanical forepump. The background pressure was in the range of $p = 10^{-5}$ to 10^{-7} torr. The use of the system was discontinued once the dc magnetron sputtering apparatus became available. The main reasons for abandoning the dc diode sputtering were:

1. Difficulty in maintaining a sufficiently low background pressure, and a higher probability of incorporating impurities from the sputtering gas (Ar) and the chamber walls, especially in view of the

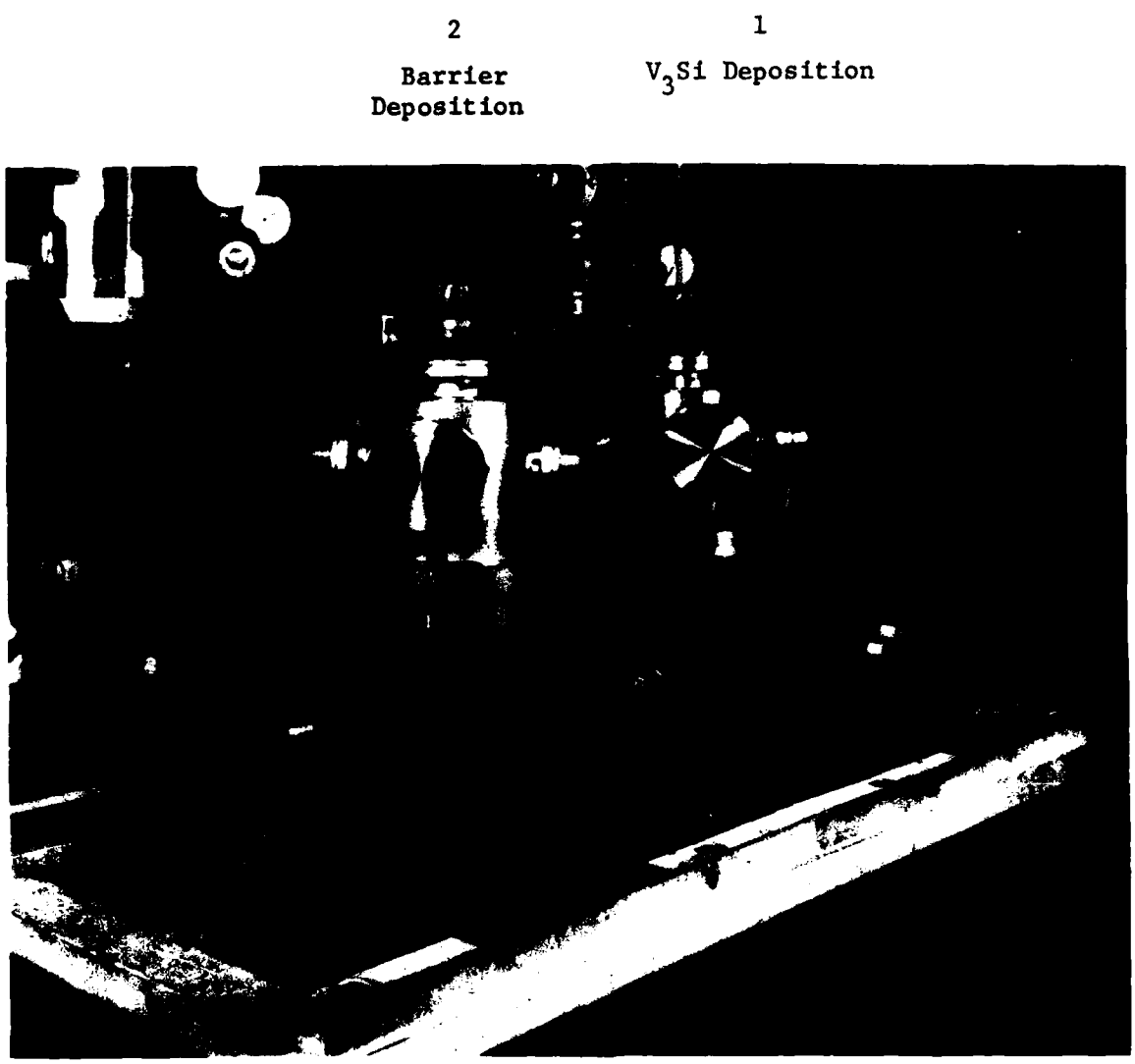

Figure 2.1 The dc diode sputtering chamber with two sputtering heads.

inherently low deposition rate.

2. Exposure of the barrier to the energetic plasma, and a concern that it might contribute to the barrier damage due e.g. to ion beam mixing.

3. Difficulty in controlling the A15 (V-Si) deposit composition over a multiple sample area when using elemental split targets (see Section 3.1), (this difficulty could have been obviated by the use of powder-metallurgical or arc-cast targets).

The dc diode sputtering method had also been used in conjunction with the thermal decomposition (pyrolysis) of silane gas (SiH_4) to *in situ* fabricate V_3Si/Si bilayers. In this case a separate small dc diode sputtering apparatus was equipped with a V target, a gas ($Ar+SiH_4$) pre-mixing chamber, and a low thermal mass heater permitting one to change the sample temperature much faster than in the case of the apparatus of Fig. 2.1. The sapphire substrates were placed directly on the heater, without clamping. The target to substrate spacing was $\sim$1.9 cm. The background pressure was typically $p \simeq 10^{-6}$ torr. The silane had been bled into the plasma zone during V sputtering to produce V-Si deposits. Upon completion of sputtering the gas supply was cut off and pumped out thus terminating both the plasma and the pyrolysis process. The temperature of the heater was then reduced, the sputtering power supply turned off, and SiH_4 injected again to deposit the Si overlayer. The necessary time interval between the V-Si deposition cut-off and start of the overlayer deposition was approximately 3 minutes.

2.2 The DC Magnetron Sputter Apparatus

The dc magnetron sputtering apparatus was constructed to become a part of the Superlattice Facility (SF, Section 2.3). It can, however, be used independently and it has been operated to date in that mode. The general view of the system in its present state is shown in Figure 2.2.

The deposition chamber shown schematically in Figure 2.3 is $\sim$30 cm in diameter. It is equipped with two "US Inc." Model 200 planar magnetron guns, water cooled, and modified for UHV operation by the manufacturer. The magnetron gun requires a disk target, 5 cm in diameter and

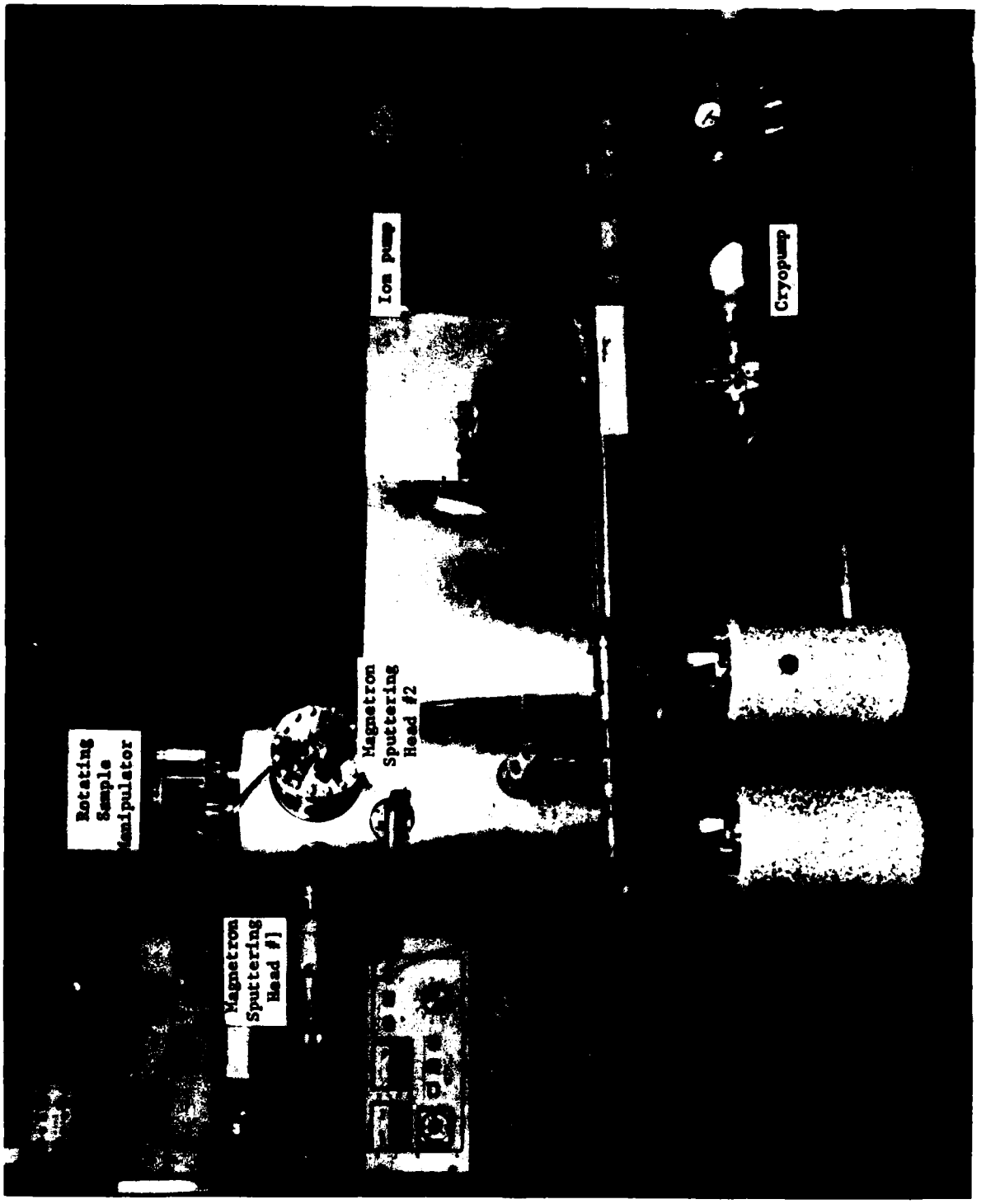

Figure 2.2 The dc magnetron sputtering chamber.

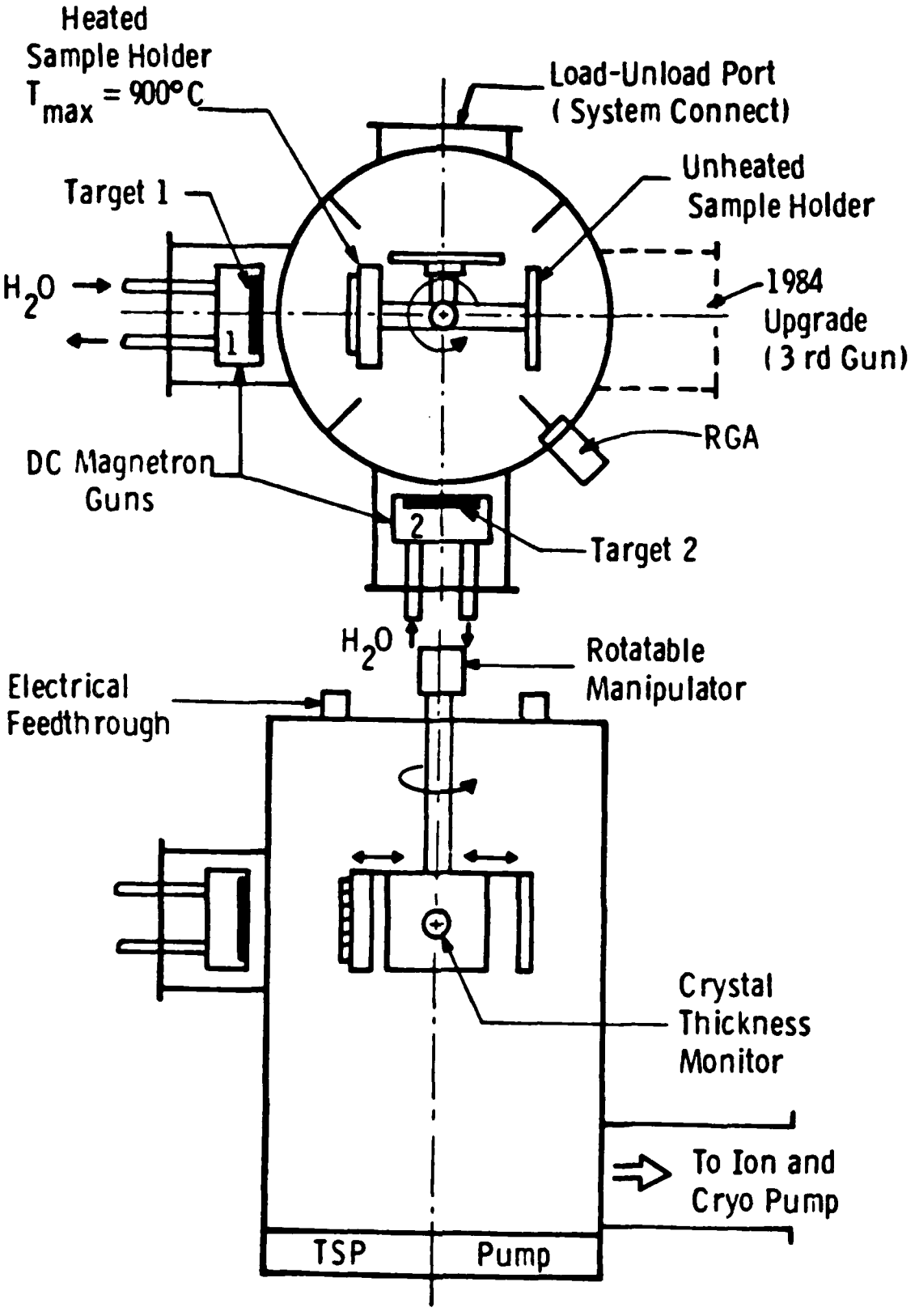

Figure 2.3 Top view and front view schematic drawings of the dc magnetron sputtering chamber.

up to 0.3 cm thick, ground flat to insure adequate heat sinking to the water-cooled mount. Two sample holders, one heated up to 950°C, another unheated, are mounted on a manipulator that can be rotated ≥360° about the vertical axis. Each holder accommodates a molybdenum block to which 8 substrates 6 x 6 mm are clamped in vertical plane. The temperature of each block is monitored by a chromel-alumel thermocouple. A separate position on the manipulator is provided for the quartz crystal thickness monitor that permits one to approximately determine the deposition rate as a function of the target-to-sample distance, and of other deposition parameters. The target-to-sample (or crystal monitor)distance is adjustable, and typically set at ∿7.5 cm. The deposit thickness uniformity specified by "US Inc," is ±5% over a 5 cm diameter area at a distance of 12 cm from the gun. The superconducting film deposition is being performed with the substrate block facing one gun. Subsequently, the manipulator is turned 90° for the block to face the second gun and the overlayer is deposited.

The system is pumped by an ion pump, a titanium sublimation pump (TSP) and a cryopump (Varian) to achieve a background pressure of 0.5 to 2 x 10^{-8} torr after baking with the sample holder at 900°C. During sputtering the ion pump is isolated, TSP inactive, and pumping is performed by the throttled cryopump.

The system will have to be somewhat modified prior to the connection to the Superlattice Facility (SF). A Riber transfer rod will be installed for transfering from and to the SF lock (loading) chamber. Sample holders and mounting blocks will be replaced to achieve compatibility with Riber, and to reduce the thermal inertia. Eventually, the chamber will be equipped with three sputtering guns for trilayer fabrication, and will have an additional port with a device for fast sample cooling after the base electrode deposition. A residual gas analyzer(RGA) and, possibly, a reflection high energy electron optics (RHEED) will eventually be attached. The latter will necessitate, however, a two-level rotating manipulator to be installed.

2.3 The Superlattice Facility

The thin film deposition and analysis system by "Riber" (France) is a state-of-the-art, metal gasketed, ultra-high vacuum facility incorporating the three functions of substrate preparation (load lock), film deposition, and surface analysis into three interconnected but isolable subsystems. A fourth subsystem is represented by the magnetron facility described in the previous section, and connectable to either the sample preparation or film deposition chamber. This is schematically shown in Figure 2.4. The substrate is moved between vacuum chambers of the subsystems by remote transfer mechanisms so that the sample is not exposed to ambient atmosphere between operations. Each of the functional subsystems has its own independent pumping and pressure monitoring system, including liquid-nitrogen-cooled titanium sublimation pumps, capable of reducing chamber pressure, after baking, into the 10^{-11} torr range (except for the load lock).

The sample preparation chamber has facilities for pre-deposition conditioning of the substrate and post-deposition film treatment. These include an ion milling/sputter cleaning gun and a substrate heater for substrate degassing or vacuum annealing at temperatures up to 1200°C.

The deposition subsystem chamber has three independent electron beam gun sources and two temperature-controlled Knudsen effusion cells, all simultaneously operable and separated by liquid nitrogen cooled baffles, to allow sequential deposition, co-deposition, and doping on rotating substrates heated in the temperature range up to 1200°C. A stationary cryogenic stage (-150°C) is also provided. Deposition rate control of up to two E-beam evaporated elements simultaneously is presently provided by a dual-head light absorption rate meter, ("Sentinel" by Inficon) and is checked by quartz crystal monitors. Electrically operated shutters (main and individual element) control individual layer or total film thickness. Many operations are monitored and controlled by the system computer. A residual gas analyzer provides data on background gas levels. These gas levels are minimized during deposition by

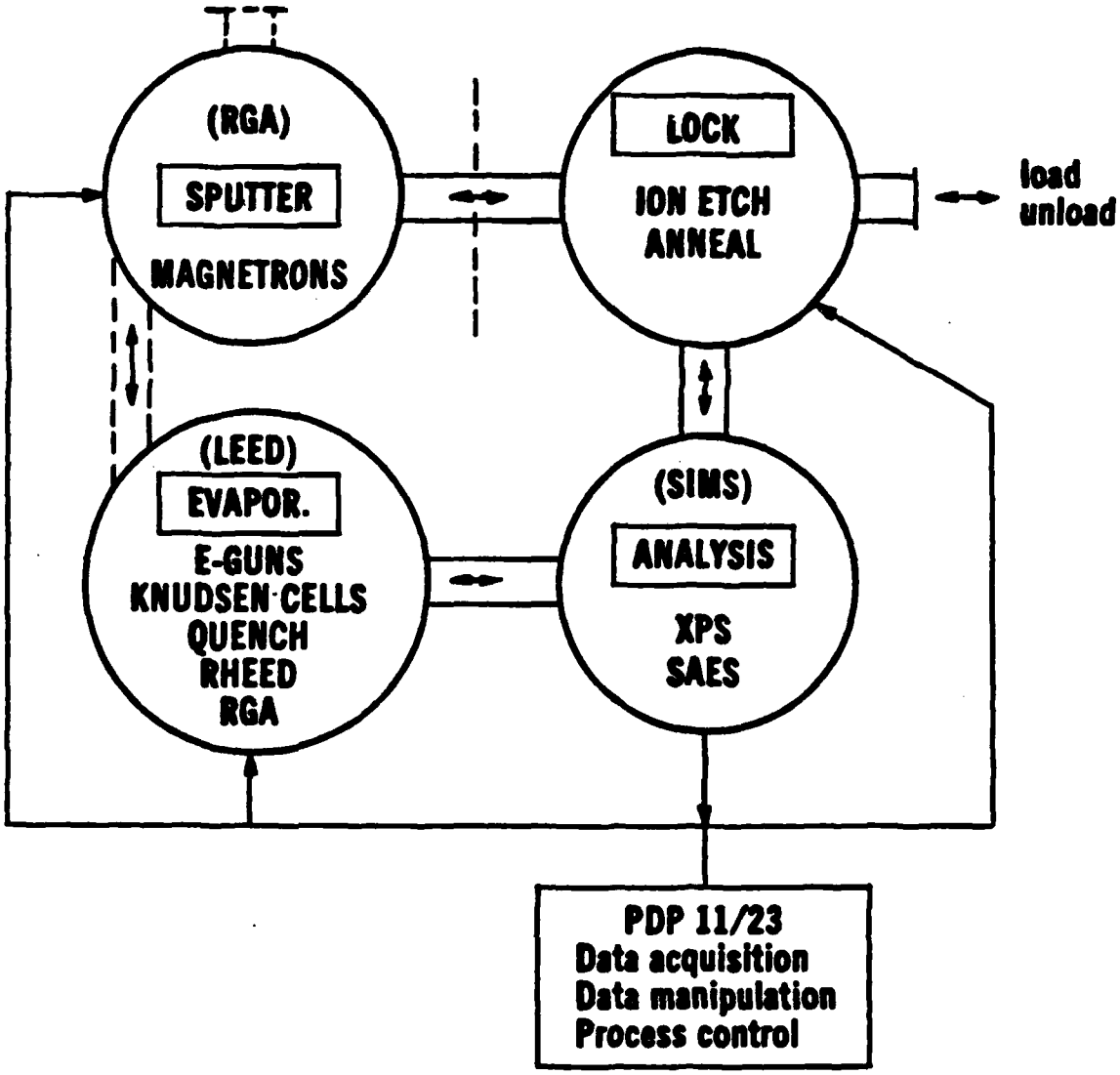

Figure 2.4 Schematic drawing of the Superlattice Facility Anticipated upgrading of the system is indicated by broken lines and brackets.

extensive liquid nitrogen cooled baffling which reduces surface heating and resulting gas desorption. This is especially important when refractory metals are being evaporated onto hot substrates. Reflection high energy electron diffraction capability is built into the deposition chamber for monitoring of deposit crystallinity and epitaxial growth. A port for low energy electron defraction (LEED) upgrade is also provided.

The surface analysis subsystem chamber has a precision manipulator with heatable substrate stage, a differentially pumped ion gun for profiling, an electron gun (ten micron spot size), dual x-ray source, and analysis optics for Auger Electron Spectroscopy (AES) (including sample imaging capability) and Photoelectron Spectroscopy for Chemical Analysis (ESCA) or XPS. The chamber is designed to permit system upgrading by addition of Secondary Ion Mass Spectrometry (SIMS).

The system includes a mini-computer (PDP 11-23) with 20 megabyte hard disc storage and peripherals for deposition control and acquisition and reduction of surface analytical data.

The system was tested in France by Westinghouse personnel during most of September, 1983. Figure 2.5 shows the general view of the vacuum chambers under test. Most specifications were met, however, with one important exception. The "Sentinel" rate monitor and the electron-beam evaporation source electronic feedback control circuit proved incapable of attaining the required automatic evaporation rate control of ±1 at.% of niobium. Depending upon its level the rate was fluctuating ±7 to ±20 at.%. *A significant upgrade work will have to be performed by Westinghouse before Nb-based A15 films such as Nb_3Ge could be deposited with adequate composition control.* There are reasons for believing that the vanadium evaporation rate control will be more accurate, so that V-based A15's could be fabricated even before the upgrade. Evaporation of Mo-Re will not be dependent upon the rate controllers. Consequently, it is hoped that the present program will not be adversely affected by the rate control problem.

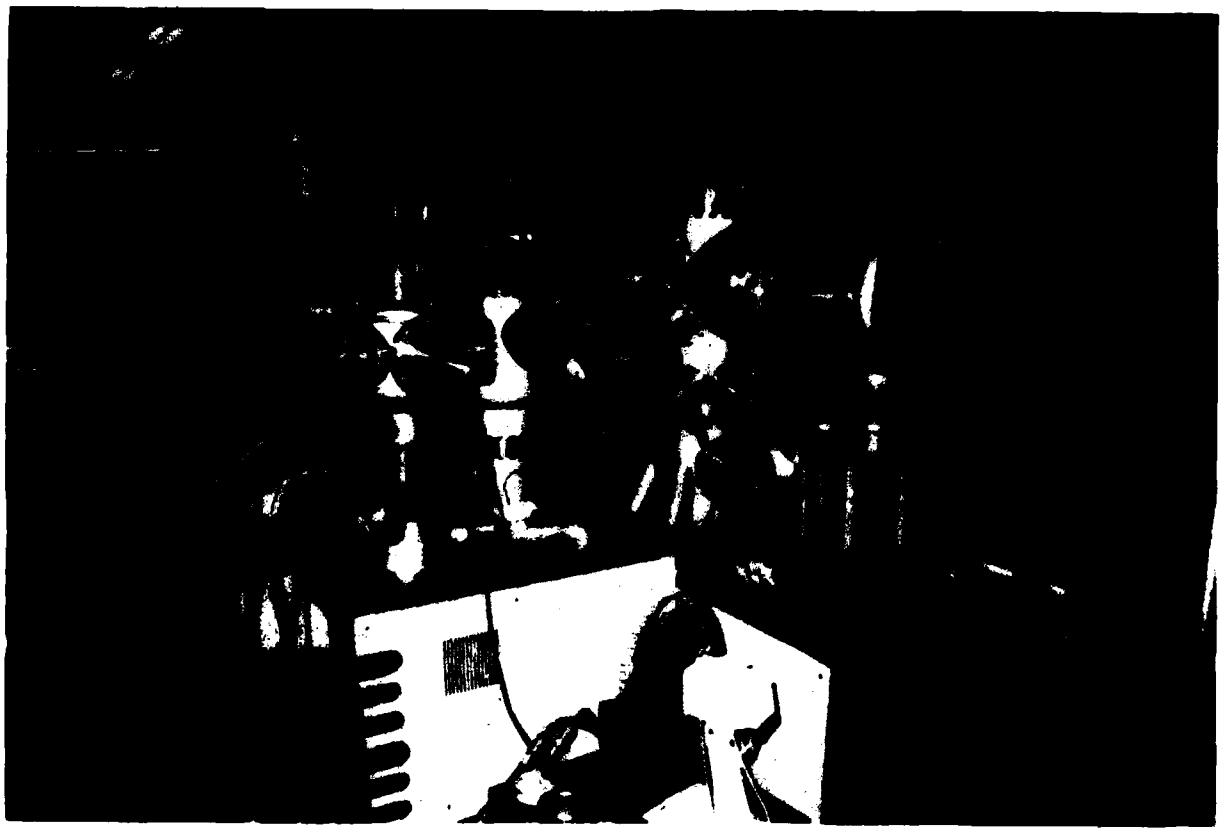

Figure 2.5 The Superlattice Facility during testing in France. The introduction chamber, analysis chamber, and evaporation chamber are positioned from left to right in this perspective.

The system was delivered to the Westinghouse R&D Center on October 5, 1983, and it is presently assembled by Riber's personnel. It is expected that the system will become operational by the end of 1983.

2.4 Analytical Methods

The XPS investigations were carried out in an ESCALAB Mark II (VG) with a hemispherical electron energy analyzer. The $Mg_{K\alpha}$ X-rays were used in all cases without a monochromator. All the films analyzed were on sapphire substrates and were not electrically grounded. Consequently, shifts in the binding energy up to 10eV could be expected. Since the films were exposed to air, however, enough carbon was found on the surface to calibrate all other photoelectron energies to the C_{1s} peak at a binding energy of 284.6 eV. High resolution spectra were recorded with an analyzer pass energy of 20 eV which corresponds to 1.2 eV resolution. The angle between the normal to the sample and the detector, θ, is defined to $\pm 6°$ because the entrance aperture of the analyzer subtends a 12° arc. The typical operating vacuum level was 10^{-9} to 10^{-10} torr.

A scanning electron microscope (Cambridge MK 150-2) equipped with an analyzer (Kevex 7000) for energy dispersion spectroscopy (EDS) and an electron microprobe capable of measuring oxygen content have been used for determining chemical composition. An x-ray diffractometer (Scintag PAD 2) has been used for phase identification and lattice constant measurement.

2.5 Sample Geometry and Test Equipment

All substrates used to date have been single-crystal sapphires. Both epitaxial grade sapphire surfaces and 0.5 μm polished sapphires have been used. The impact of the roughness of the film surfaces on artificial barrier properties is discussed in Section 3.2. No difference in barrier properties has been found for films grown on sapphires which have been polished differently.

Figure 2.6 is a schematic drawing of a 6 mm x 6 mm chip prepared for single tunnel junction measurements. The base electrode and

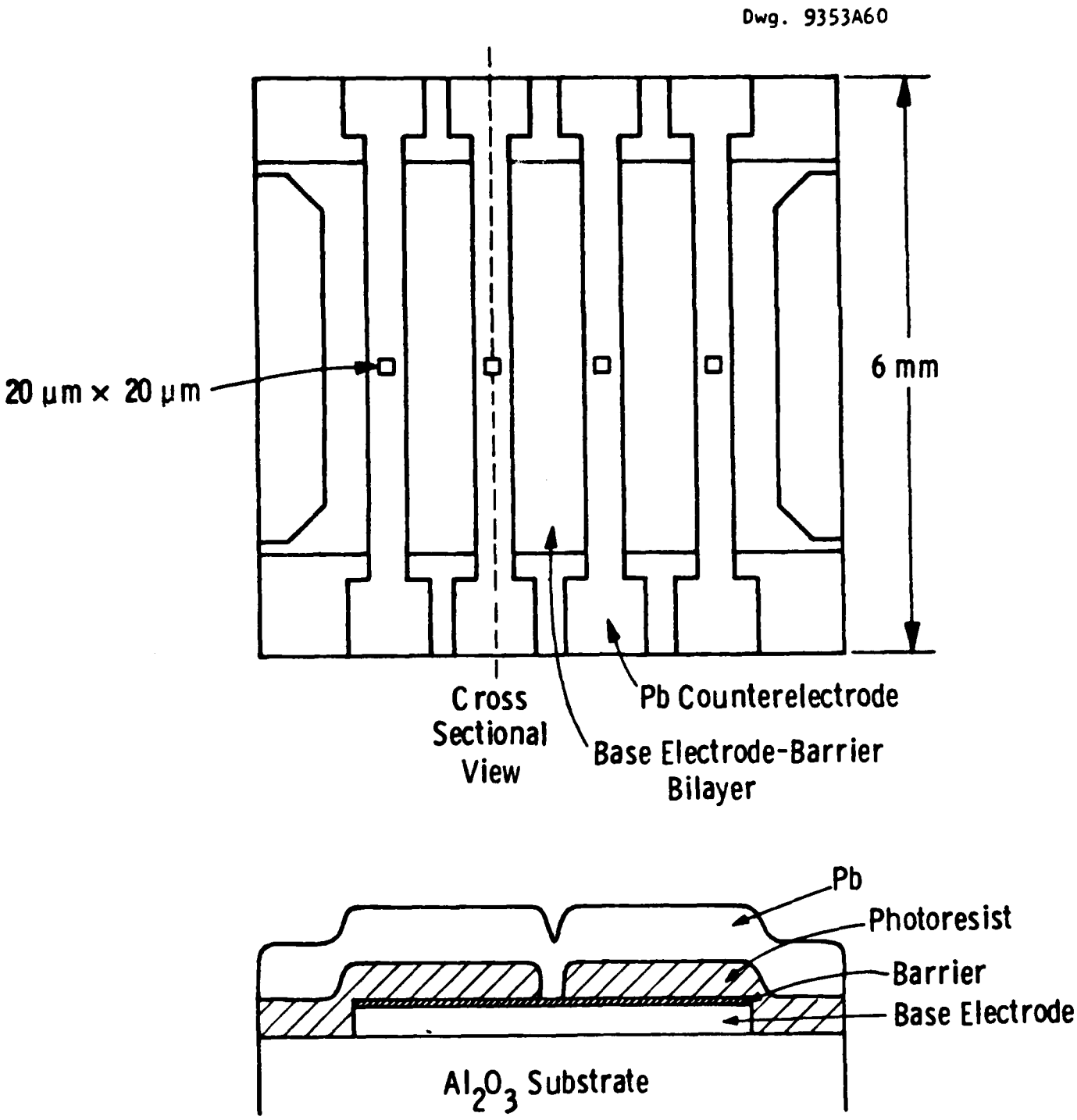

Figure 2.6 Geometry of a single 6 mm x 6 mm sample prepared for tunneling measurements in a top view and in cross section.

artificial barriers were deposited on the sapphire substrate in one of the sputtering chambers described earlier in this section. The clamps which held the sapphires to a heated molybdenum block to insure good thermal contact masked a strip 1 mm wide on two edges of the substrates.

The sample was allowed to oxidize in air for a fixed time up to 24 hours before photoresist (1350 J) was patterned to leave four 20 μm x 20 μm square junction areas exposed. Large areas have also been exposed on the edges of the substrate which permit electrical contact to the base electrode. Lead evaporated through an aperture mask was used to form counterelectrodes and contact pads for electrical connections.

Junctions have been made just as described above but without using photoresist to define the junction area when it has been necessary to process the samples quickly. The junction area was then approximately 4 mm long with a width determined by the 0.5 mm wide Pb stripe. Generally, polystyrene Q-dope was painted along the step from the sapphire to the base electrode to eliminate any effects of the step-edge.

Two probes have been modified for this program. Both have press-contact electrical connections to the sample for rapid sample turn-around. One probe permits a resistive measurement of transition temperature and van der Pauw[1] measurement of resistivity as a function of temperature in a liquid helium storage dewar with a 1/2-inch neck. An air-lock allows the sample to be warmed from cryogenic to room temperature in dry nitrogen gas.

The second probe accommodates four sapphires. Sixteen contacts are made to each chip permitting a four-point measurement of the dc properties of each tunnel junction. The temperature of the samples is controllable. An air-lock built for this probe enables the samples to be brought to room temperature in vacuum or in dry nitrogen.

2.6 Experimental Approach

The general definition of the approach is given in Section 1.2. Prior to describing the first year's results, however, it is desirable

to present the rationale for experimental choices and preferences that shaped the first year activity thus defining the detailed approach to date, and the extent to which specific tasks have been addressed.

Base Electrode Materials

In the original Westinghouse proposal (No. 82M435) V_3Si was chosen as the base and counterelectrode material representative of stable A15 high-T_c compounds. The Nb_3Ge was chosen as the highest-T_c representative of the metastable A15's to be investigated in later years, once the stable A15 will be in hand. Finally, the Mo-Re alloy that can also crystallize as A15 but has a T_c relatively independent of long-range order was chosen as the backup material to be investigated for the counterelectrode use.

At the inception of experimental work the decision was made to include in the initial study (Tasks 1 through 3 of the Work Statement, Section 1.1) the Nb base electrode, in addition to V_3Si and Mo-Re. The rationale for this extension of the scope of work was to have a reference material permitting one to compare own results with those already published by other authors. By mid-1982 no data existed on the surface oxidation properties of A15's while Nb had been investigated extensively.[2] Analytical data existed on the oxidation of bi-layers consisting of the base electrode coated by a thin metallic overlayer[3] only for Nb. Also more numerous and detailed data existed on tunneling into niobium with artificial barriers than into A15's. In the case of tunneling into V_3Si only the evaporated and oxidized SiO_x barrier had been investigated.[4,5]

Barrier Materials

The originally proposed (82M435) barrier material was an oxidized rare-earth metal represented by Y_2O_3. This choice was based primarily on the very high oxygen affinity of rare earths. No literature information was then available on the Y_2O_3 barrier, and only preliminary tunneling results on other rare earth (Er, Lu) barriers studied with soft (Pb, In) counterelectrodes had been reported.[6]

The SiO_x and Al_2O_3 ($Al\ O_x$) were included here as reference barrier materials. All the initial choices were retained during the first year of work. By the end of 1982 and in early 1983 some data became available on yttrium overlayers.[7,8] It is known that the use of a yttrium oxide barrier results in problems when a Nb-counterelectrode is used. The tentative explanation proposed is based on the observed formation of yttrium hydroxide that apparently seals the pinholes but is removed, thus permitting shorts, by high-oxygen affinity counterelectrode.[8] This issue has not yet been resolved by others nor addressed here. Consequently, there was no strong reason thus far to alter the barrier material choices.

Tunnel Junction Patterning

Task 2 of the work statement (Section 1.1) specified the development of a selective anodization process for A15 films. This task was formulated based on the analogy with the selective niobium anodization process (SNAP) developed at Sperry Research Center for Nb/Si/Nb junctions.[9] A process permitting patterning of the counterelectrode after the *in situ* fabrication of a base/barrier/counterelectrode trilayer will be highly desirable or even necessary, especially in the case of an epitaxial growth of the counterelectrode. The development of a SNAP analogy thus appeared appropriate. Private information from Sperry obtained at the beginning of the program made it clear, however, that the anodization process does not work well for Nb compounds such as NbN. At the same time a successful demonstration of the trilayer counterelectrode patterning by reactive plasma etching of niobium (SNEP) was reported by Bell Laboratories.[10] Since the parameters of this process are generally less sensitive to the type of material processed than in the case of anodization, a decision was made eventually to switch from the SNAP to a SNEP-type process. This required, however, acquisition of a plasma etching apparatus that only now became available. Consequently, Task 2 was not addressed during the first year of this program.

Tunneling

Study of the fabrication of tunnel junctions with Pb, soft alloy or Nb-counterelectrode was initially envisaged (82M435) to start in the second half of first year and to continue into the second year (Task 3, Section 1.1). The soft or Nb-counterelectrode was to be used to establish a reference base for comparison with data available from literature. The analytical and tunneling studies were thus to be conducted sequentially. At the inception of work it became clear, however, that the significance of analytical results would be enhanced if correlated with tunneling data on a continuing basis. Consequently, work on Tasks 1 and 3 started at the same time and continued throughout the year. Thus far, only Pb-counterelectrode has been used.

3. RESULTS AND DISCUSSION

3.1 Superconducting Electrode Material Properties

Niobium

Niobium base electrode films had been initially deposited by dc diode sputtering. Once the dc magnetron equipment (Section 2) became available in May of 1983 work continued using this sputtering method. The dc magnetron results are emphasized here since this deposition method is expected to be used in conjunction with the Superlattice Facility for the duration of this program.

All niobium films prepared by magnetron sputtering have been deposited in 5×10^{-3} torr of argon. The typical background pressure with substrates heated to 500°C before introducing argon was 5×10^{-9} torr. Films deposited at both T_d = 500°C and at ambient (no heater) temperature showed a sharp resistive transition at temperatures between 9.0 and 9.3K with the precise value more dependent on background pressure than on substrate temperature. At T_d = 500°C the niobium resistivity ratios were between Γ = 10 and 12 while ambient temperature samples had ratios of 3 to 4. Slightly higher T_c and Γ were obtained with a deposition rate of 6 Å/sec than with 2 Å/sec. In initial runs the ambient temperature of the molybdenum substrate holder was rising steadily during a 2 Å/sec deposition from a poorly-cooled target to 140°C in a half hour. Present work with a water-cooled target indicates that the substrate remains at below 70°C even at higher sputtering rates up to 6 Å/sec. Sputtering time was adjusted in each case to produce Nb films between 0.2 and 0.4 μm thick.

The properties of the niobium films produced by dc diode sputtering were less reproducible than those which were deposited by magnetron sputtering. The onset of superconductivity was 9.2K for all films deposited at T_d = 500°C but the transition width varied from 0.1 to 0.8K and Γ from

3 to 8. Films deposited at room temperature were not superconductors. The sputtering voltage was 2000V with an argon pressure of 0.40 torr for a rate of 12 Å/sec.

The surface oxidation of niobium has been investigated and is discussed here to introduce the technique of evaluating the XPS data. Figure 3.1 includes Nb_{3d} XPS spectra from a Nb film which had been exposed to air for a cumulative time of approximately three days. The exciting X-rays were $Mg_{K\alpha}$ radiation and the energy analyzer was perpendicular to the film. The native oxide thickness can be calculated by comparing the intensity of the chemically shifted peak characteristic of the oxide with the intensity of the unshifted peak. The film is modeled as having a smooth layer of oxide of uniform thickness, d, on top of unoxidized metal. The intensity ratio permits a calculation of d/λ where λ is the photoelectron escape depth.[3] In the case of Nb_{3d} photoelectrons,

$$\frac{I_{Nb_2O_5}}{I_{Nb}} = \frac{1 - e^{-d/\lambda \cos \theta}}{e^{-d/\lambda \cos \theta}} \qquad (1)$$

The angle, θ, is defined by the direction of the electron detector and the normal to the films. The intensities must be scaled by sensitivity factors supplied by the manufacturer of the electron analyzer (VG-ESCALAB) for the pure elements. For alloys or compounds such as Nb_2O_5 the intensity also has to be scaled by the number density of Nb in the oxide compared to the number density in the pure metal. Finally, the intensity ratio should be scaled by the photoelectron escape depth if markedly different for the metal and its oxide. This difference is neglected in the present work and one value of λ is assumed.

The accuracy of the calculation depends on the uniformity of the top layer thickness, the ease with which overlapping peaks in the spectrum can be separated, and an appropriate choice of λ. The uniformity of the top layer will be addressed in the discussion of artificial barriers. The magnitude of the chemical shift due to a highest valency oxide such as Nb_2O_5 is usually large enough compared to the peak width to enable the

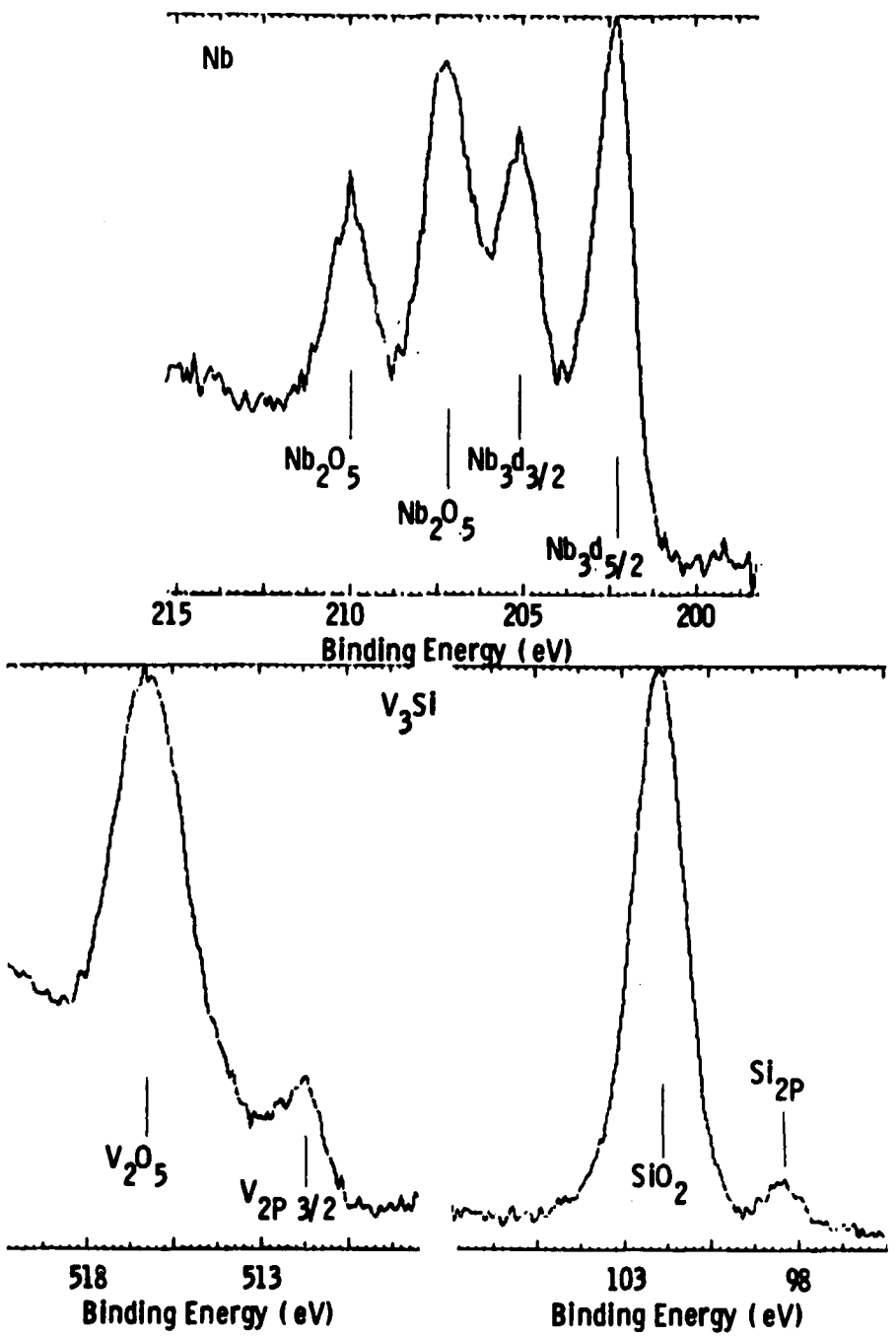

Figure 3.1 XPS spectra recorded for native oxides grown on niobium and vanadium silicon.

separation of peaks for elements of concern with the exception of vanadium. The $V_{2p\,3/2}$ peak from V_2O_5 overlaps the satellites of O_{1S} due to $Mg_{K\alpha 3}$ and $Mg_{K\alpha 4}$ X-ray lines as well as the $V_{2p1/2}$ peak from metallic vanadium. Quantitative work with vanadium oxide is therefore least accurate. Chemical shifts due to lower oxides (e.g. NbO_2, NbO) are in general more difficult to resolve.

A value for the escape depth of λ = 20 Å will be used in this report for all materials. This is a reasonable value based on numbers in the literature.[11,12] It will be shown that it gives a good agreement between nominal barrier thicknesses and calculations based on equation (1). Table 3.1 includes the thickness of native niobium oxide formed in air. The value calculated from XPS data using equation (1) is compared with a value from the literature. The reference thickness is reported for three days exposure to air but does not represent a saturation of oxide growth. The 24 Å thickness measured from Figure 3.1 also resulted from exposure to uncontrolled humidity air for three days. *It will be measured again to look for saturation of the oxide growth.* No attempt was made here to resolve the Nb XPS spectra for the presence of lower oxides and suboxides underneath the Nb_2O_5 surface layer. It was shown in the literature, however, that NbO and NbO_x ($x \simeq 0.02$) are usually present. The latter case extends to depths comparable to or exceeding the thickness of Nb_2O_5.[2] The NbO is a superconductor with a $T_c \leq 1.5K$ and at 4.2K represents a proximity layer. The NbO_x ($x \simeq 0.02$) is a degraded superconductor. Both are expected to affect tunneling through the native Nb_2O_5 barrier. Examples of the successful use of a thermal Nb oxide to form tunnel junctions are rare.[13] In the present study, attempts to make tunnel junctions by depositing a Pb counterelectrode on air-oxidized Nb resulted in shorts.

Vanadium Silicon

The V-Si films had been initially fabricated by dc diode sputtering and since May, 1983 by dc magnetron sputtering using the apparatus described in Section 2. As in the case of niobium, the magnetron results are emphasized here and are presented first.

Table 3.1
Native Oxide Thicknesses

Material	Oxide Thickness (Å)		
	XPS	Literature	
		Value	Ref. No.
V_3Si V	66	13	11
V_3Si Si	78		
Nb	24	24	2
MoRe Mo	2	--	
MoRe Re	1	--	
Y	> 100	--	
Al	25	30	25, 26

The V-Si has been magnetron-sputtered from a sintered powder metallurgical target purchased from a commercial source (Materials Research Corp.). Such targets have been selected to achieve composition uniformity over a deposit area 3 to 4 cm. in diameter. They typically contain 0.5 to 1.0 at.% oxygen determined by electron microprobe analysis and are formed of a rather coarse V and Si powder mixture. This coarseness permitted, at least initially, a selective removal of silicon due to its higher sputtering rate. Arc cast, homogeneous targets would be greatly preferred but the formidable difficulty of machining brittle A-15 disks to the close tolerances required to insure adequate heat sinking in the sputter gun (Section 2) could not be overcome, so far. *Further work aimed at fabricating low impurity content targets with better than 1.0 at.% film composition control will be performed.*

The properties of magnetron-sputtered V_3Si films used as a base electrode are summarized in Table 3.2. Sputtering conditions were 60W of dc power, 15×10^{-3} torr argon, and a rate of 0.7 Å/sec. The background pressure of 2×10^{-8} torr was somewhat higher than for niobium depositions since the substrate temperatures were higher. The substrate temperature for run 8 was 850°C and was 900°C for all the other runs. The resistivity ratio, Γ, was lower for run 8 due to the lower substrate temperature. The resistive transition temperature width was 0.1 to 0.2K for all but the last sample. Reproducibility of T_c and Γ was good from one run to the next as well as within a single deposition up to run 15. The target had cracked from being heated too quickly and by run 15 some material from the backing plate sputtered through the cracks to contaminate the films and lower the T_c by 0.5K. A new V_3Si pressed-powder target is now in place.

The T_c values correspond to those of bulk samples of V_3Si with 24 at.% silicon.[14] X-ray diffractometer scans of samples from runs 11 and 16 showed an A-15 structure with no V_5Si_3 phase. The lattice constant was 4.725 Å which corresponds to 25 at.% Si in the A-15 material.[14] The pressed powder target contained nominally 24.7 at.% Si. These indications

Table 3.2

V_3Si Properties, DC Magnetron Sputtering

Run	Sample	Base Thickness (μm)	T_c (5% to 95%)	Γ (ρ_{300}/ρ_{20})	at. % Si	
					XPS	EDS
M83-8	B2	0.20 *	14.4 to 14.6	3.7	64	29
M83-8	B3	0.20 *	14.4 to 14.6	3.7	--	--
M83-8	B4	0.20 *	14.4 to 14.6	3.5	75	--
M83-10	B3	0.24	14.5 to 14.6	4.5	29	--
M83-11	B3	0.31	14.5 to 14.5	4.2	26	32
M83-12	B4	0.31	14.7 to 14.8	4.6	31	--
M83-13	B4	0.32	14.4 to 14.6	4.4	29	--
M83-14	B4	0.32	14.5 to 14.6	4.7	25	--
M83-15	B3	0.32	14.1 to 14.6	3.7	--	32
M83-16	B3	0.32	13.8 to 14.1	3.3	33	--
$V_{75.3}Si_{24.7}$ target scrape-cleaned just before analysis					24	26.8

*No artificial barrier

that the V-Si films contain ⩽25 at.% Si have not yet been reconciled with the composition measured by standardless EDS (Table 3.2) which probes the top several thousand angstroms of material.

The silicon composition at the surface of the film measured by XPS is shown in Table 3.2. Silicon is the only element which has an XPS sensitivity factor calibrated for the energy analyzer used here.[15] That sensitivity factor was used for silicon and the manufacturer's (VG Scientific) value was used for vanadium in compiling Table 3.2.

The samples of run 8 are the only V_3Si films without an artificial barrier on top. Sample 8-B2 was exposed to air with an uncontrolled humidity for 3 days prior to XPS analysis. The native oxides, V_2O_5 and SiO_2, were 66 Å and 78 Å thick (Table 3.1). Ihara et al.[11] observed an oxide layer of only 13 Å when V_3Si is in a dry oxygen atmosphere for a similar length of time. They reported that a silicon-rich surface layer forms as a preliminary step to oxidation. After the oxide has grown, there is still a silicon-rich layer underneath although no numbers are reported for the composition of the layer. The surface layer of sample 8-B2 was 64 at.% silicon in qualitative agreement with Ihara. The samples of run 8 contained 29 at.% silicon determined by standardless EDS which measures the composition of the bulk of the film. The XPS measurement was repeated for sample 8-B4 which had been warmed from 4.2K to room temperature in humid air with no effort to prevent water from condensing on it after its T_c had been measured. The surface appeared tarnished and the XPS spectra confirmed that the surface oxide is >100 Å thick. No XPS peaks corresponding to metallic V_3Si were observed. The composition of the surface layer was 75 at.% silicon (with respect to vanadium). The thicker oxide was, therefore, more silicon-rich than the surface oxide of sample 8-B2.

The surfaces of the V_3Si samples of runs 10 through 16 were protected by artificial barriers. However, there was still a thin layer of both V_2O_5 and SiO_2 observed by XPS. The origins of the oxide layer will be discussed in the next section in connection with Table 3.3. The surface composition of the V_3Si underlayer was enriched by only 1 to 9 at.% silicon compared to the clean V_3Si target. Measurements of the V-Si sur-

face composition under thicker barrier layers will be done to see if the surface segregation can be completely eliminated when there is no oxidation of the V_3Si.

Diode-sputtered V-Si films have been fabricated in the so-called phase-spread configuration from a split target formed of two elemental pieces - V and Si. This was the standard method used at Westinghouse for A-15 thin film formation over the past 10 years. The typical conditions were voltage: 800 V, current: 100 mA, argon pressure: 0.70 torr, deposition temperature 875°C. The V-Si films typically had a T_c onset of 16K, a ΔT_c = 0.5K, and a $\Gamma \approx 6$ for the best sample from each run. However, the split target resulted in a composition spread of 15 at.% silicon across the four 1/4-inch long substrates. An effort was made to reduce the composition spread by using up to five strips of silicon across a vanadium target. Unfortunately, there was a higher sputtering rate from edges compared to flat surfaces and from silicon compared to vanadium. During the run silicon was redepositing on the vanadium parts of the target. These effects combined to result in films with a composition that was initially unpredictable and not reproducible. This form of diode sputtering was abandoned once the magnetron sputtering apparatus became available for reasons stated in Section 2.

Reactive diode sputtering utilized a 0.71 torr sputtering gas which consisted of 0.6% SiH_4 in argon. The vanadium target was sputtered at 830 V, and 100 mA for a deposition rate of 1 to 2 Å/sec. There was a composition spread across the samples with silicon-rich samples located closer to the gas inlet. The substrate temperature was 800°C during the V_3Si deposition. The sputtering gas was pumped away and the high voltage turned off to end the V_3Si deposition. After the 3 minutes needed to cool the substrates to 310°C, the gas mixture was introduced again to deposit a silicon barrier at 6 Å/min. This process may be extended to reactive magnetron sputtering if initial experiments are successful.

Molybdenum Rhenium

The following two tasks related to the anticipated use of Mo-Re as a high-T_c counterelectrode have been addressed:

1. Determine the lowest substrate temperature in dc diode sputter-deposition from a powder-metallurgical target.
2. Verify the ability of dc magnetron sputtering from a powder-metallurgical target to reproduce earlier, high-T_c results obtained by Gavaler *et al* using dc diode sputtering and metallic, split targets.[16]

(1) An available powder-metallurgical target of nominal composition $Mo_{86}Re_{14}$ was used to deposit films by dc diode sputtering at various substrate temperatures T_d. The T_c onset obtained as a function of T_d is shown in Fig. 3.2. All samples exhibited transition widths of about ΔT_c=1K. The transition temperature is normalized to T_c=6.3K obtained at T_d=900°C. This value is in agreement with data for bulk $Mo_{86}Re_{14}$,[17] and somewhat lower than the 8 to 9K obtained by Gavaler when using a metallic target.[16] At the lowest deposition temperature of T_d=60°C, obtained by cooling the sample holder with liquid N_2, the T_c was ~6.0K, only 5% below the reference value. For pure Mo-Re the amorphous-crystalline transition, T_{a-c}, is only ~120K[18] but the effect of impurities such as oxygen on this transition is not known quantitatively. Qualitatively, one should expect T_{a-c} to increase with the concentration of impurities. The results of Fig. 3.2 show that the impurity concentration resulting from the use of a sintered Mo-Re target did not prevent adequate crystallization at a temperature presumably low enough to avoid tunneling barrier damage by thermally-activated diffusion during Mo-Re counterelectrode deposition. The sintered targets typically contain 0.5 to 1.0 wt.% O_2 as determined by electron microprobe.

(2) The magnetron deposition results in a lower kinetic energy of incoming atoms than the dc diode sputtering. Hence, the barrier damage by energetic particles during the counterelectrode deposition will be less likely to occur. Consequently, a sintered target of nominal composition

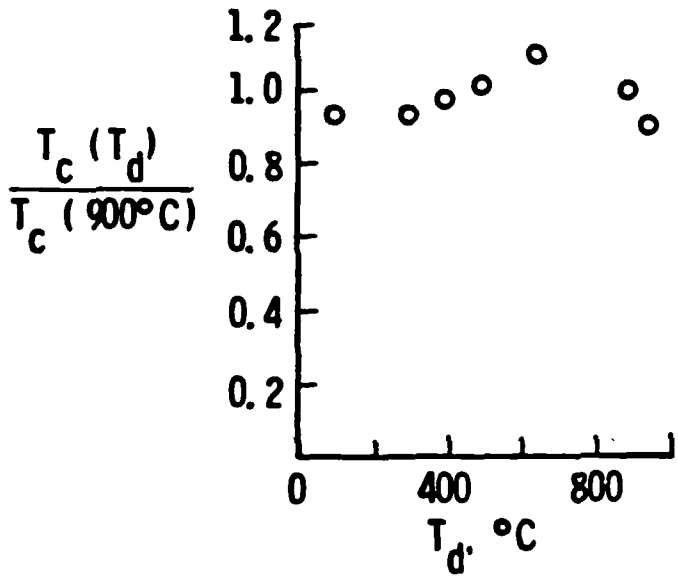

Figure 3.2 The superconducting transition temperature of $Mo_{86}Re_{14}$ as a function of substrate temperature, T_d.

$Mo_{65}Re_{35}$ is being used to deposit high-T_c films by dc magnetron sputtering. Standardless electron microprobe analysis of this target indicated $Mo_{70}Re_{30}$ with ~0.5 wt.% oxygen.

The T_c expected for bulk $Mo_{65}Re_{35}$ is about 12K.[17] Gavaler obtained up to T_c=15K for films which were dc diode sputtered from a split metallic target with T_d=1000°C and a deposition rate of 8 Å/sec.[16] Three magnetron deposition experiments were performed to date using a comparable rate of 7 Å/sec. According to EDS measurements, the films only contain 23 to 24 at.% Re. Bulk samples with this composition have a $T_c \approx$ 9.5K.[17] The two sets of samples deposited at T_d= 875°C and 900°C had sharp resistive transitions ($\Delta T_c <$ 0.1K) at 9.0 and 9.2K. The resistivity ratios were 2.2 and 2.5 corresponding to background pressures of 4×10^{-8} and 7×10^{-9} torr before introducing argon at 15×10^{-3} torr for sputtering. Films made at ambient temperature, T_d=70°C, with a background pressure of 7×10^{-9} torr were not superconducting in a measurement down to 4.2K.

An accurate determination of the target composition will be made using X-ray fluorescence. The target will then serve as a standard for EDS measurements of film composition.

The Mo-Re/overlayer oxide bilayers have not been fabricated since no high-T_c films were obtained to date. From the discussion to follow (Sections 3.2, 3.3) it will become clear, however, that high-T_c Mo-Re base electrodes should facilitate the fabrication of high quality tunnel junctions due to the observed low oxygen affinity of Mo-Re. Such junctions could be of value as references for a comparison with A-15 based junctions.

3.2 Yttrium Oxide Barriers

All bilayers consisting of the yttrium barrier on top of a superconducting film have been prepared *in situ* by dc magnetron sputtering as discussed in Section 2. The deposition rate was $\sim$ 17 Å/min. The cumulative oxidation time in air of uncontrolled high humidity (summertime) at room temperature was approximately 24 hours.

Table 3.3 includes a compilation of the bilayers which have been fabricated and characterized. The nominal barrier thickness is determined from a sputtering rate measured on a much thicker deposit with a stylus-type profilometer. The barrier thickness determined by XPS is based on a comparison of peak areas using equation (1). Figure 3.3 shows part of a survey spectrum containing Nb_{3d} and Y_{3d} peaks for 16 Å and 40 Å of yttrium on niobium. The large qualitative difference in the relative peak heights indicates that the choice of a particular type of background subtraction or smoothing routine does not significantly change the information gained from such a measurement. When the artificial barrier is a third element deposited on V_3Si, one can calculate the barrier thickness by comparing the count rate from the third element with either vanadium or silicon. In such a case both results are tabulated.

The yttrium peaks of Figure 3.3 analyzed at higher resolution as well as spectra from yttrium on V_3Si such as in Figure 3.6 showed no metallic yttrium. All yttrium barriers studied to date have been completely oxidized before XPS analysis or counterelectrode formation.

The most striking feature of Table 3.3 with regard to yttrium overlayers is the agreement between the nominal and XPS-measured barrier thicknesses. The only exception is for the samples with a nominal thickness of 54 Å on Nb and is a significant one because the Nb was at T_d = 250°C while the Y was deposited. Several of the other Nb/Y bilayers had Y deposited at 40°C because the Nb was deposited at ambient temperature. The 250°C substrate temperature was chosen as a maximum when the base electrode was formed at much higher temperatures. It represents a compromise which is well below temperatures at which thermal diffusion would

Table 3.3

Barrier and Oxide Thicknesses, Nominal and by XPS

Bilayer Materials	Nominal Barrier Thickness (Å)	Barrier Thickness from XPS (Å)		Barrier Substrate Temp. (°C)	Base Electrode Oxide Thickness from XPS, Å
		DC Magnetron Sputtering			
Nb/Y	7	--		40	--
	16	17		230	2
	27	31		40	6
	40	39		40	1
	54	24		250	6
		V/Y	Si/Y		
V_3Si/Y	10	11	10	230	9
	20	31	26	240	8
	35	44	37	250	6
V_3Si/Al	5	10	8	250	29
	13	--	--	210	--
	20	24	22	200	6
	37	27	20	150	16
		DC Diode Sputtering			
Nb/Si	18	16		< 200	25
	40	--		< 200	--
	45	--		< 200	--
V_3Si/Si	18	--		< 200	--
	40	$\lesssim$ 23		< 200	< 1
	42*	$\lesssim$ 43		$\geqslant$ 300	< 1
	50	--		< 200	--
	55	$\leqslant$ 31		< 200	< 1

*Barrier by SiH_4 decomposition

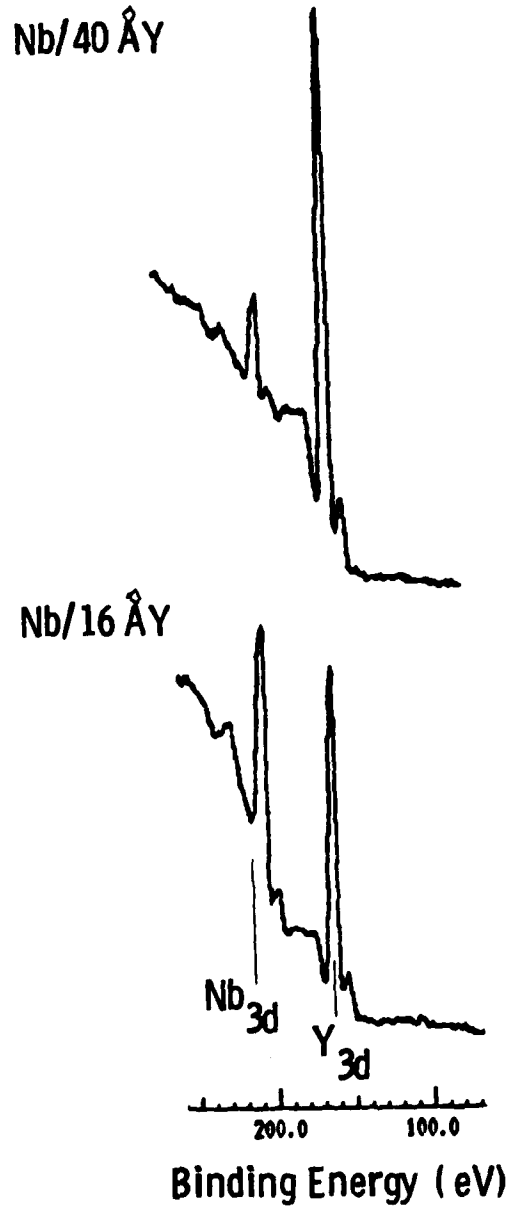

Figure 3.3 Relative XPS peak heights for two Nb/Y bilayers.

affect the interface and yet minimizes the time the interface is exposed to impurities before depositing the barrier. Rudman found some decrease in tunneling properties when he deposited silicon barriers on V_3Si at temperatures above 300°C.[19] *A new substrate holder with a lower thermal mass is soon to be installed in the magnetron chamber. This should allow for more freedom in the choice of barrier deposition temperatures without excessive exposure of the interface.*

The 24 Å thick barrier which was nominally 54 Å thick can be interpreted as a confirmation of a result reported by Kwo et al[3] where they attribute the missing material to loss by grain boundary diffusion. These authors did not observe, however, any barrier material loss in the case of a very thin (12 Å) Al_2O_3 barrier. Table 3.3 provides again an analogy whereby no loss is observed for a 16-17 Å yttrium barrier on Nb in spite of a high T_d = 230°C. The fact that loss is observed only for thicker layers is qualitatively consistent with the proposed wetting mechanism[20] but a detailed interpretation is not available at this point. The correlation of T_d and loss for thicker barriers is in any case clearly demonstrated. The Nb/Y bilayer with 40 Å of yttrium shows that there is no loss of material if the base electrode is at room temperature even though the room temperature niobium has a smaller grain size than that formed at 500°C.

There is no analogous loss of material for the 35 Å yttrium barrier formed on V_3Si at 250°C. This leads to the speculation that Y wets Nb better than it wets V_3Si. Miedema's theory[20] does not allow one to draw such an inference if one assumes that V_3Si-Y wetting properties are defined by V and Y alone. There is, however, no theoretical insight into the wetting of binary compounds. Also, wetting is very strongly reduced by the presence of impurities. The residual gas pressure, higher in the case of V_3Si than in the case of Nb, might be a sufficient cause for reduced wetting. More evidence of the tendency of a barrier material to completely cover the base electrode can be found by analyzing the oxidation of the base electrode in the bilayer samples in conjunction with tunneling results.

Figure 3.4 shows the type of dc tunneling characteristics obtained with fully-oxidized yttrium barriers on either niobium or V_3Si. Sample 7-C3 has a nominal barrier thickness of 27 Å on niobium. The subgap conductance is so high that the sumgap, $\Delta_{Nb} + \Delta_{Pb}$, is somewhat obscured. However, $\Delta_{Nb} + \Delta_{Pb} = 2.6$ mV at 4.2K is the expected value. This particular junction area was defined by crossing a strip of Nb/Y with a strip of Pb without using photoresist or Q-dope to further limit the junction area. The possible sources of such large leakage currents for V_3Si junctions are numerous but for niobium junctions there is apparently only one difference between these barriers and the barriers of Kwo et al[7] which result in high quality tunnel junctions. The difference is that in junctions fabricated here the barrier is completely oxidized, and the base electrode has at least a small amount of oxide. Junctions prepared at Bell Laboratories show no oxidation of the underlying niobium and a small amount of unoxidized Al[3], Mg, or Y[7] if the deposited overlayer exceeds a certain minimum nominal thickness. These overlayers are deposited on a rotating substrate to enhance the uniformity of coverage.

There are three different effects which would lead to the oxidation of the base electrode.

1. One expects a barrier of uniform thickness less than the native oxide thickness reported in Table 3.1 to eventually oxidize completely and thus expose the base electrode to oxygen. It is obvious that this case applies to the Y barriers which are all thinner than the 100+Å of native oxide. Figure 3.5 shows the larger V_2O_5 peak of oxide formed under 10 Å of Y compared with that formed under 35 Å of Y. The thickness of the oxide can be calculated if it is modeled as a uniform layer on top of the unoxidized metal. The results of such calculations based on equation (1) are listed in the last column of Table 3.3. The barrier protects the Nb or V_3Si to the extent that the oxide is always thinner than the native oxide would be without the barrier. The base electrode oxide is generally thinner under the thicker barriers.

This effect will be separated from other causes of base electrode oxidation by depositing thicker yttrium barriers and limiting their exposure to air before XPS analysis and counterelectrode deposition.

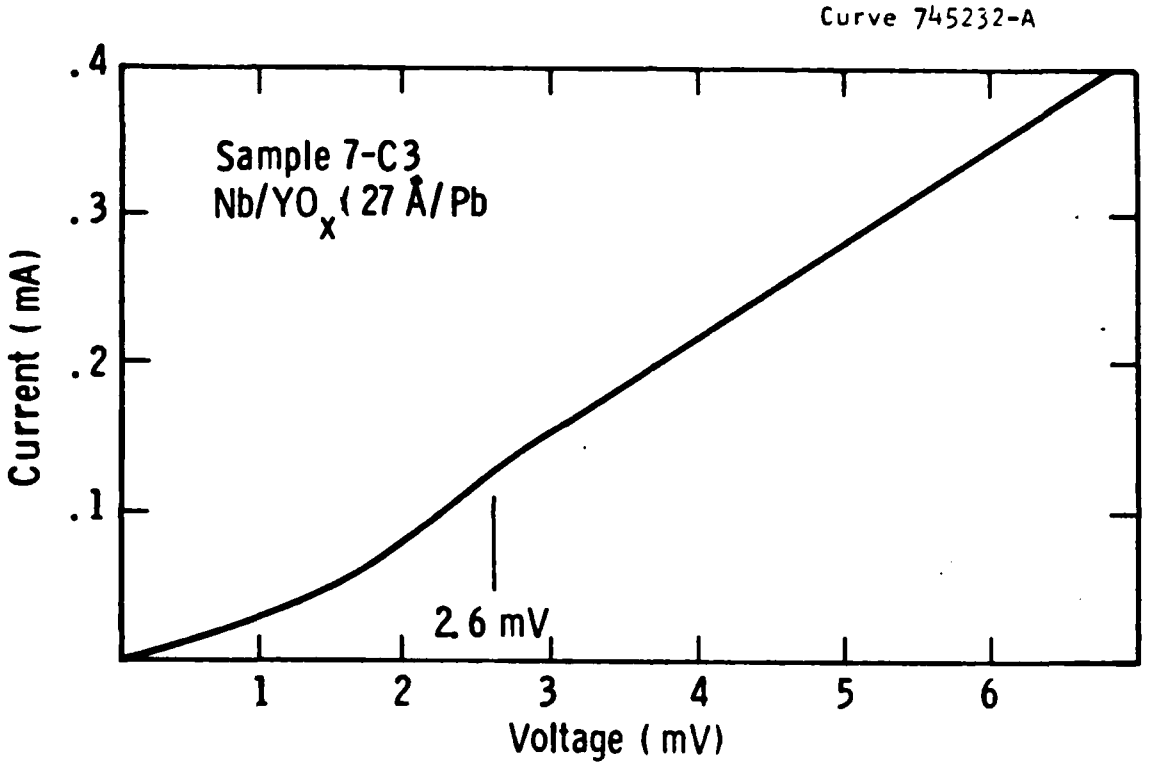

Figure 3.4 The dc tunneling characteristics of a Nb/YO$_x$/Pb junction.

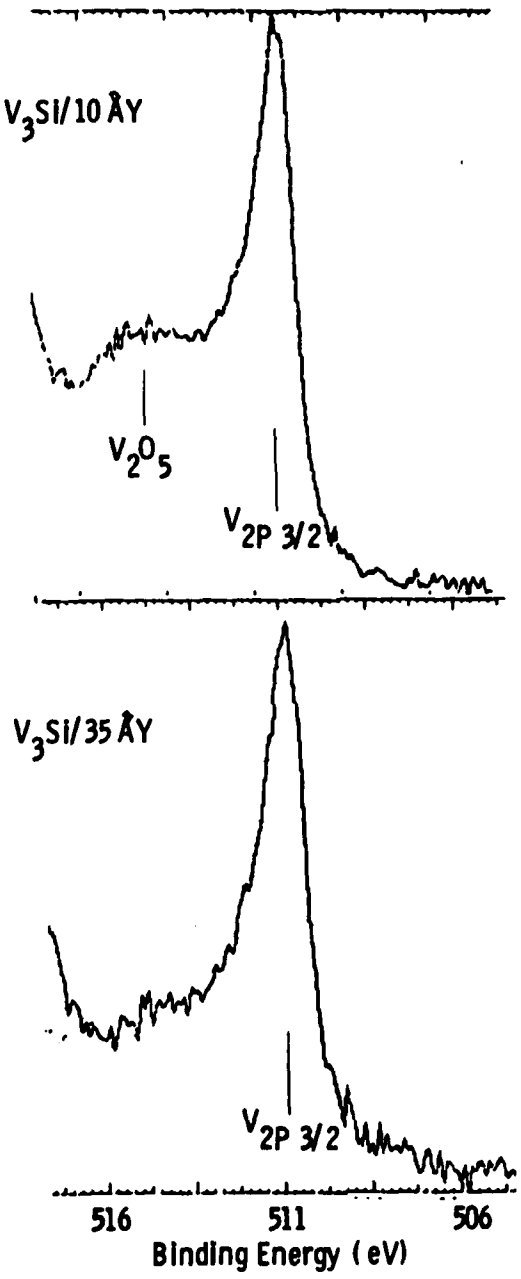

Figure 3.5 The oxidation of vanadium with yttrium barriers 10 Å and 35 Å thick.

The sample with a 35 Å Y overlayer on V_3Si was measured by XPS after 15 minutes in air, but the yttrium had completely oxidized. *Further experiments will limit the exposure to less than 5 minutes.*[7] Such short exposure times are possible when defining crude junction geometries but make more sophisticated patterning impossible. This is one more motivation to move to a completely *in situ* process immediately after high quality single junctions can be made with Pb counterelectrodes.

2. A second possibility which would lead to oxidation of the base electrode is an uneven or incomplete coverage by the barrier material. XPS measurements have also been made with the detecting angle 10° (θ=80°) from the surface of the film to study this effect. At this angle, the number of photoelectrons from the base material decreased relative to those from the barrier, but not as much as it would if there was a smooth and uniform barrier layer. The thickness of the barrier determined by a comparison of peak areas is about a factor of 4 less than the data in Table 3.3 taken with the detector perpendicular to the film. There are two causes considered in detail by Grundner.[21] First, a rough surface would have some facets exposed to the detector which are nearly normal to the detector's direction for any θ. The second possibility is that the barrier coverage is incomplete or uneven leaving some of the base material at or near the surface. The films studied in this project are 0.2 to 0.4 μm thick and polycrystalline so the surface is certainly rough compared to the scale of the barrier thickness. However, roughness alone should correspond to a glancing angle spectrum identical to the normal angle spectrum. For these films, the base electrode shows more oxidation when studied at a glancing angle. Therefore, the barrier thickness is uneven either due to the roughness or some other property such as the wetting tendency of an overlayer which has already been discussed.

Grundner has studied niobium native oxides on rough (0.1 μm) niobium surfaces. He observed a decrease by a factor of 3 between d(θ=0) and d(80°) for the thickness of the oxide on electropolished niobium. He has used simple models for the effects of roughness and non-uniform thickness

of the top layer. Each of the two models has a distinctive d (θ) curve which can result in d (0°)/d (80°) = 3 with the appropriate model parameter. A measurement of the complete d (θ) curve is a time-consuming but straightforward procedure. *This measurement will be performed to evaluate the uniformity of the Y and Al barriers.*

3. If incomplete or non-uniform coverage is not detected then the remaining possibility is that of some base electrode oxidation occurring prior to the barrier deposition on base materials grown at high T_d. The typical cooling time for the substrates was 20 minutes. In a vacuum of 10^{-8} torr, only 2 minutes are needed to expose the surface to a monolayer of impurities. The cooling time can be reduced with a new substrate holder as was mentioned in the context of limiting the diffusion of the barrier material into the grain boundaries of the base electrode.

The cooling time may not be as important when the barrier is yttrium or aluminum which both have a stronger oxygen affinity than niobium or vanadium. The barrier material would tend to reduce the surface of the base electrode. The reduction of submonolayer amounts of NbO by Y has been observed by Kwo et al.[7]

Two papers dealing with the surface analysis and barrier properties of yttrium oxide, Y_2O_3, and yttrium hydroxides of unknown stoichiometry, $Y(OH)_x$ were mentioned in Section 2.6.[7,8] A splitting of the O_{1s} XPS peak was observed when artificial barriers of metallic Y on Nb were oxidized in air. A similar double peak for O_{1s} has been observed in this work for all the Y layers. No evidence of such a double peak has been found for barriers of oxidized Al or Si or for any native oxide studied except Y (Table 3.1) so the second peak cannot be due to suboxides of the base electrode.

Figure 3.6 shows the O_{1s} spectra for three V_3Si/YO_x bilayers. The hydroxide O_{1s} peak was shown by Ronay and Latta[8] to be at a higher binding energy (+∿ 2.5 eV) than the oxide O_{1s} peak. Therefore, one expects the hydroxide peak of Y_{3d} photoelectrons to be at a lower binding energy than the oxide Y_{3d} peak. The shift could be, however, much less than 2.5 eV since the transfer of a fixed amount of electronic charge affects the binding of each element differently.

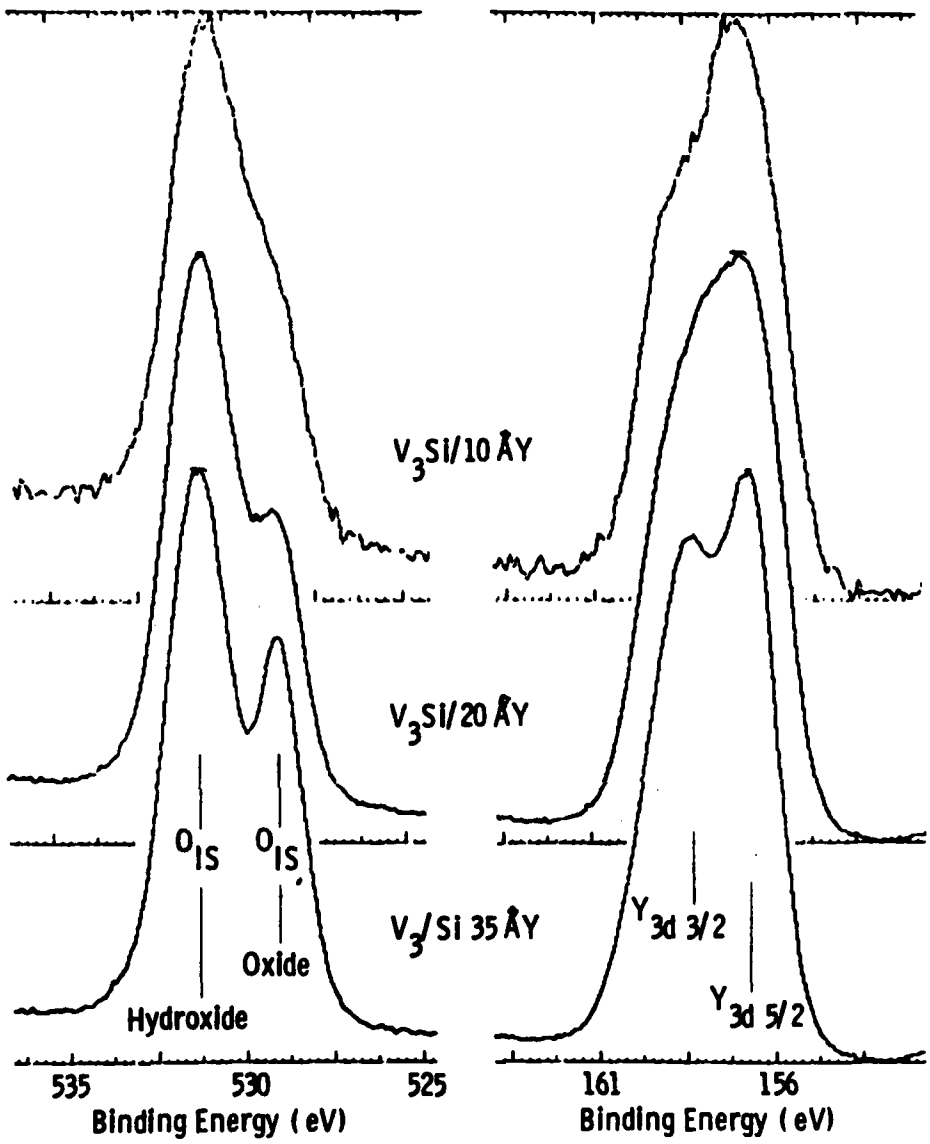

Figure 3.6 Yttrium oxide and hydroxide content of 10, 20 and 35 Å yttrium barriers.

Kwo et al.[7] presented Y_{3d} spectra which suggested the presence of overlapping peaks on both sides of the central doublet. The lower binding energy peak was from metallic yttrium, the higher energy peak was interpreted as being due to $Y(OH)_x$, and the central $Y_{3d5/2}$ and $Y_{3d3/2}$ doublet was from Y_2O_3. The argument presented above for the sign of the chemical shift from oxide Y_{3d} to hydroxide Y_{3d} means the central doublet should have been due to $Y(OH)_x$ and the higher energy peak due to Y_2O_3.

The Y_{3d} peaks shown in Figure 3.6 indicated that in samples investigated here there was no metallic yttrium, and no obvious sign of a higher energy peak overlapping the central doublet. However, there was a shift in the relative peak heights from $Y_{3d3/2}$ to $Y_{3d5/2}$ as thinner Y barriers were examined. There should be a ratio of 4:6 for the areas of these two peaks if the doublet represented a single environment for Y. The apparently shifted weight toward the $Y_{3d5/2}$ peak for thinner samples has two interpretations although only the latter might be consistent with the trend for the O_{1s} peak and with Kwo's data (with the relabeling of $Y(OH)_x$ and Y_2O_3 peaks suggested above):

1. The increased height of the $Y_{3d5/2}$ peak for thinner barriers could simply be due to a broadening of both peaks in the doublet as suggested by the computer subtraction of spectra. The peak separation was 1.75 eV so the resolution of the instrument (1.2 eV) would separate sharp peaks from a well-ordered material. It is reasonable that the disorder which resulted in broadened peaks would be greatest for the thinnest barrier where all yttrium atoms are within a monolayer of an interface with vacuum (atmosphere) or V_3Si. The shift between oxide Y_{3d} and hydroxide Y_{3d} would have to be negligible for this explanation. Kwo's data for nearly equal amounts of Y_2O_3 and $Y(OH)_x$ showed that the Y_{3d} shift is on the order of 1 eV.[7]

2. The increased height of the $Y_{3d5/2}$ peak for thin barriers could also be due to the shift of some of the yttrium from an oxide to a hydroxide environment. While this is consistent with the O_{1s} data, the fraction of material shifting from oxide to hydroxide must be

consistent for the O_{1s} and Y_{3d} peaks. *A peak synthesis and separation procedure will be done to obtain these quantitative results.*

A conclusion to be drawn from either case 1 or 2 is that the barrier has an uneven distribution of yttrium oxide and hydroxide with more hydroxide on the surface. Early glancing angle (θ = 80°) XPS measurements seemed to lead directly to this same conclusion. However, many of the O_{1s} photoelectrons were coming from the edge of the Al_2O_3 substrate. With the use of an appropriate aperture which eliminated the effect of the substrate, the θ = 80° spectra were similar to the θ = 0° spectra for each sample.

The yttrium barriers were all exposed to humid air so the Y_2O_3 apparently grew faster than the yttrium hydroxide. However, there were indications that yttrium hydroxide growth continues for several days. Measurements of yttrium on niobium showed more hydroxide for samples exposed for three days than for one day. The native oxide on a thick yttrium deposit was measured after three days' exposure and showed a symmetric but slightly broadened O_{1s} peak with a binding energy corresponding to yttrium hydroxide.

The above discussion, although inconclusive at this point, defines the issues and difficulties in interpretation that must be resolved for a successful use of Y-overlayer-type barriers with high-T_c A15 counterelectrodes other than Mo-Re. Data of Table 3.1 show that Mo-Re has a much lower affinity to oxygen than V_3Si, Nb, and, presumably, Nb-based A15s. The Mo-Re should be an easy-to-use high-T_c counterelectrode in Y-barrier junctions if the interpretation of the hydroxide role proposed by Ronay and Latta[8] is correct.

3.3 Aluminum Oxide Barriers

All bilayers with an aluminum overlayer listed in Table 3.3 have been prepared *in situ* by dc magnetron sputtering on a base electrode of V_3Si at a rate of 10 Å/min. XPS measurements, not included in Table 3.3, have also been performed on one sample with a nominal Al barrier thickness of 78 Å on top of niobium prepared in an rf sputtering system which will generally not be used for this project since it is not a UHV system. The results for this one sample illustrate the effects of a short oxidation period on a thick barrier. It was exposed to air for 10 minutes while the thinner Al barriers on V_3Si were exposed to air for 24 hours before XPS measurements and Pb counterelectrode formation. XPS peak areas for the Nb/Al bilayer showed 18 Å of Al_2O_3 on top of 6 Å of metallic Al with no oxidation of the Nb underneath. The Al layers on V_3Si were completely oxidized and the underlying V_3Si was oxidized to a depth recorded in the last column of Table 3.3.

Figure 3.7 includes XPS data from an intermediate step (8 minutes) in the oxidation of the thinnest Al barrier, and after one day of accumulated oxidation time. The Al was completely oxidized after 8 minutes in air, and the V_3Si was oxidized to a depth of 14 Å. After 24 hours, the oxidized V-Si layer had grown to 29 Å. It would be interesting to see if such a thin barrier (nominally 5 Å; 8 to 10 Å by XPS) provided complete coverage of the V_3Si. The exposure to oxygen before XPS analysis would have to be shortened to a time on the order of a few seconds to see if the V_3Si remain unoxidized. *The in situ XPS analysis capability of the Superlattice Facility (Section 2.3) will allow such a determination to be made in the near future.*

The barrier thicknesses determined by XPS compared with the nominal thicknesses (Table 3.3) indicate that the loss of Al by grain boundary diffusion into the base electrode reported by Kwo et al.[3] for the Nb base occurs also on a V_3Si base. The nominal thickness exceeded the XPS-determined value for the 37 Å thick Al. This is similar to the situation discussed in Section 3.2 with respect to Y on Nb where the nominal Y thickness was higher than that determined by XPS for a thick

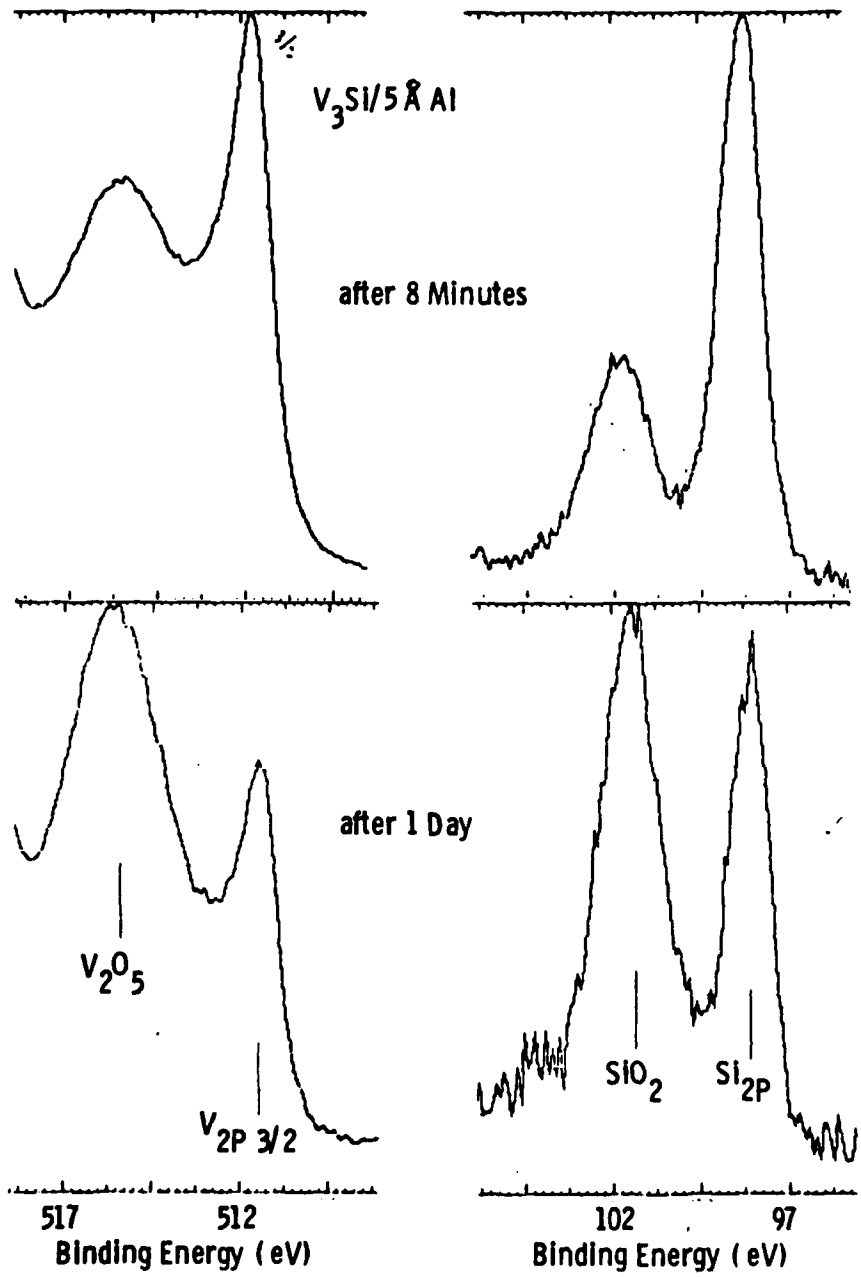

Figure 3.7 Oxidation of V_3Si after 8 minutes and after 1 day.

barrier deposited at 250°C. Unlike Al, which exhibited a loss of material when deposited on V_3Si at 150°C, a yttrium barrier of 35 Å nominal thickness deposited on V_3Si at an even higher temperature of 250°C did not diffuse into the base. This leads to the speculation that Al wets V_3Si better than Y does. Miedema's theory[20] qualitatively confirms the better wetting properties of Al on both Nb and V. The deposition of either Y or Al on V_3Si occurred at the same level of impurities so that the discussion of their possible role in reducing the wetting of V_3Si as compared to the Nb underlayer (Section 3.2) is not applicable here.

A more direct comparison with the results of Kwo et al.[3] can be made for the sample of Al which was deposited on Nb at 120°C. The 18 Å of Al_2O_3 and 6 Å of Al accounted for only 20 Å of the 78 Å metallic Al. The largest discrepancy reported by Kwo et al.[3] concerned a sample for whichonly 16 Å of Al out of a nominal thickness of 112 Å could be found by XPS analysis.

The dc electrical properties of the $V_3Si/Al_2O_3/Pb$ tunnel junctions were nearly identical to those with yttrium oxide barriers. Figure 3.8 shows one example. The expected sumgap voltage at 4.2K is 3.5 mV. The high leakage current either had the effect of masking the highest gap partially and the gap width completely or reflected the actual gap distribution from 1.3 to 3.5 mV in the top layer of the V_3Si. The surface segregation of V_3Si exposed to oxygen discussed in Section 3.2 could cause the gap degradation. The XPS measurements which determined the segregation probe the material to approximately the same depth that affects the tunneling behavior, $\xi_{GL}(0)$ = 30 to 50 Å.

However, the fact that a similar leakage was seen for dc electrical characteristics of Nb-based junctions ($\xi_{Nb}\sim$300 Å) implies that the barrier as well as the near-surface superconductor is suspect. The obvious difference between these aluminum and yttrium oxide barriers and those of Kwo et al,[3.7] is that these barriers were fully oxidized, and did not protect the superconductor surface. If an obvious reason for a leaky barrier, the incomplete coverage of the surface, caused the leakage then a longer oxidation time would be desirable to oxidize the pinholes

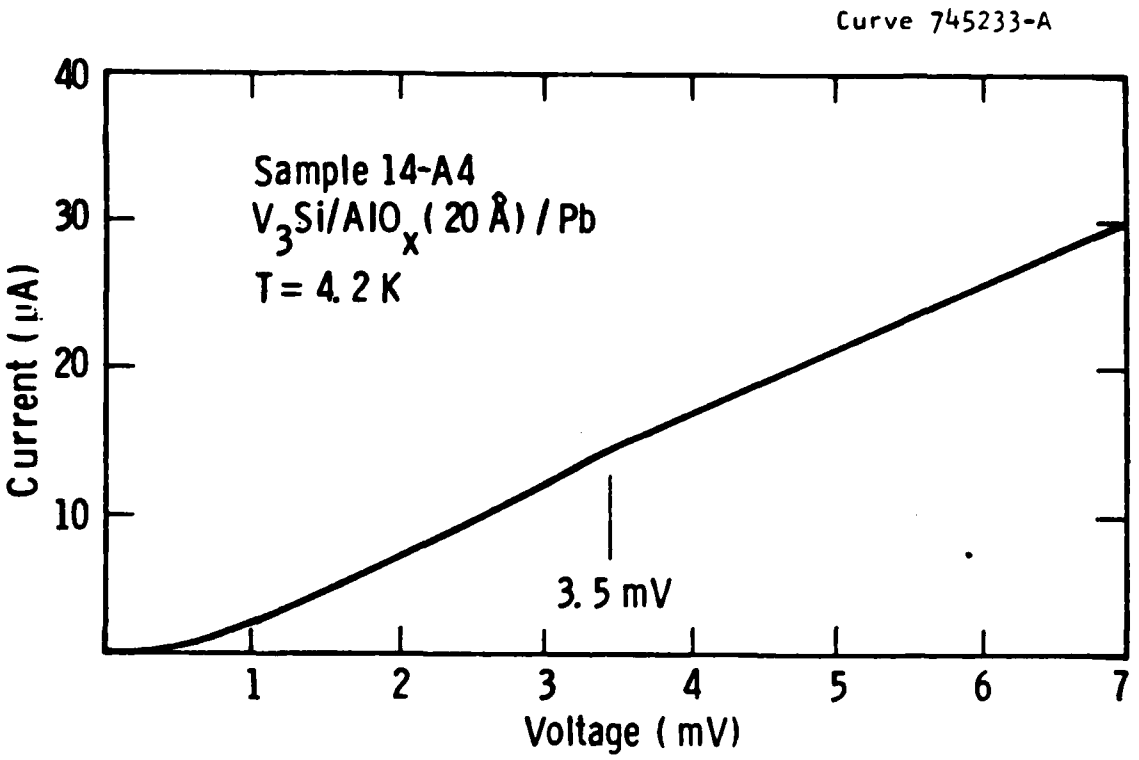

Figure 3.8 The dc tunneling characteristics of a $V_3Si/Al\ O_x/Pb$ junction.

instead of being detrimental. Theoretical explanations of leakage through a pinhole-free oxide barrier are not well-developed but one mechanism has been proposed by Halbritter.[22] His model of resonant tunneling via localized states in the oxide barrier will have to be considered when the effects of various oxidation conditions are better defined experimentally. *The first step will be to measure tunneling characteristics of junctions which do not have oxidized base electrode material at the interface with the barrier such as the one with 78 Å of Al deposited on Nb.*

The possible causes of oxidation of the base electrode which were listed in Section 3.2 are the same for Al barriers as for Y barriers. However, one difference in the ability of these materials to protect the base electrode relates to the native oxide thickness (Table 3.1). An artificial barrier of Al much thicker than 30 Å could be exposed to humid air for 24 hours without oxidizing the entire layer, in contrast to Y. The data presented earlier in this section indicate that the Al overlayer would have to be deposited on the base electrode at an undetermined $T_d << 150°C$ to permit one to use a relatively uncontrolled oxidation process.

The O_{1s} XPS spectra from the oxidized aluminum barriers had a single peak corresponding to the binding energy of Al_2O_3. The hydroxide, $Al(OH)_3$, would have a binding energy 2.7 eV higher[23] which is close to the 2.5 eV difference between yttrium hydroxide O_{1s} photoelectrons and those from yttrium oxide. No evidence of $Al(OH)_3$ was found. In the model proposed by Ronay and Latta[8] the hydroxide formed by air oxidation seals pores in the barrier thus enabling the oxidized aluminum or yttrium to be a low-leakage barrier. The deposition of Nb counterelectrode on Nb/YO_x bilayers by Ronay and Latta[8] resulted in shorts while Nb on Nb/AlO_x bilayers by Gurvitch et al. resulted in junction properties nearly as good as those of Nb/Al/Al oxide/Al/Nb junctions.[10] It appears that the role of the hydroxide is much less significant for Al than for Y-based barriers. The Al-based barriers would then be technologically more practical.

3.4 Silicon Oxide Barriers

Bilayers consisting of a silicon barrier on Nb or V_3Si were prepared *in situ* either by dc diode sputtering of both layers or by reactive sputtering of vanadium in an atmosphere of Ar-0.6% SiH_4 followed by a thermal decomposition of SiH_4 (Section 2.1). In the case of barrier fabrication by dc sputtering the deposition rate was 27 Å/min., while for SiH_4 decomposition was 6 Å/min. Following Rudman and Beasley's work with evaporated Si barriers,[4] all samples were exposed to ambient air for 24 hours before XPS analysis of the surface or deposition of a Pb counterelectrode.

Preparations were made in May, 1983, for the first samples deposited in the magnetron sputtering system to be Nb/Si bilayers. However, the pure silicon sputtering target had an electrical conductivity which was too low for dc magnetron sputtering. After experiments with Y and Al barriers were under way, a silicon target doped with 1 ppm Sb was obtained. *Experiments will continue with this new target to enable a direct comparison to be made between dc diode and dc magnetron sputtered bilayers of Nb/Si.* Samples of V_3Si/Si will not be produced until a better correlation between XPS data and high-quality tunneling barriers is found using other materials since photoelectron peaks for silicon are difficult to interpret when using this material combination.

In the last column of Table 3.3 are listed the thicknesses of niobium oxide for an 18 Å thick overlayer of silicon and a 16 Å thick overlayer of Y. The Nb_{3d} XPS spectra for the two bilayers are shown in Figure 3.9. A 25 Å layer of Nb_2O_5 was found for the first sample while 6% of the Si overlayer was unoxidized. The second sample had 2 Å of Nb_2O_5 and no unoxidized Y. The difference could be due to an intrinsic property of the two sputtering techniques, to the different wetting properties of Si and Y, or to a combination of a poor vacuum and the lower oxygen affinity of Si. Miedema's theory[20] indicates that Si should wet niobium better than Y but the poor vacuum in the diode souttering chamber was probably a dominant factor in restricting the surface mobility of silicon. XPS measurements of magnetron sputtered Nb/Si samples should resolve these possibilities.

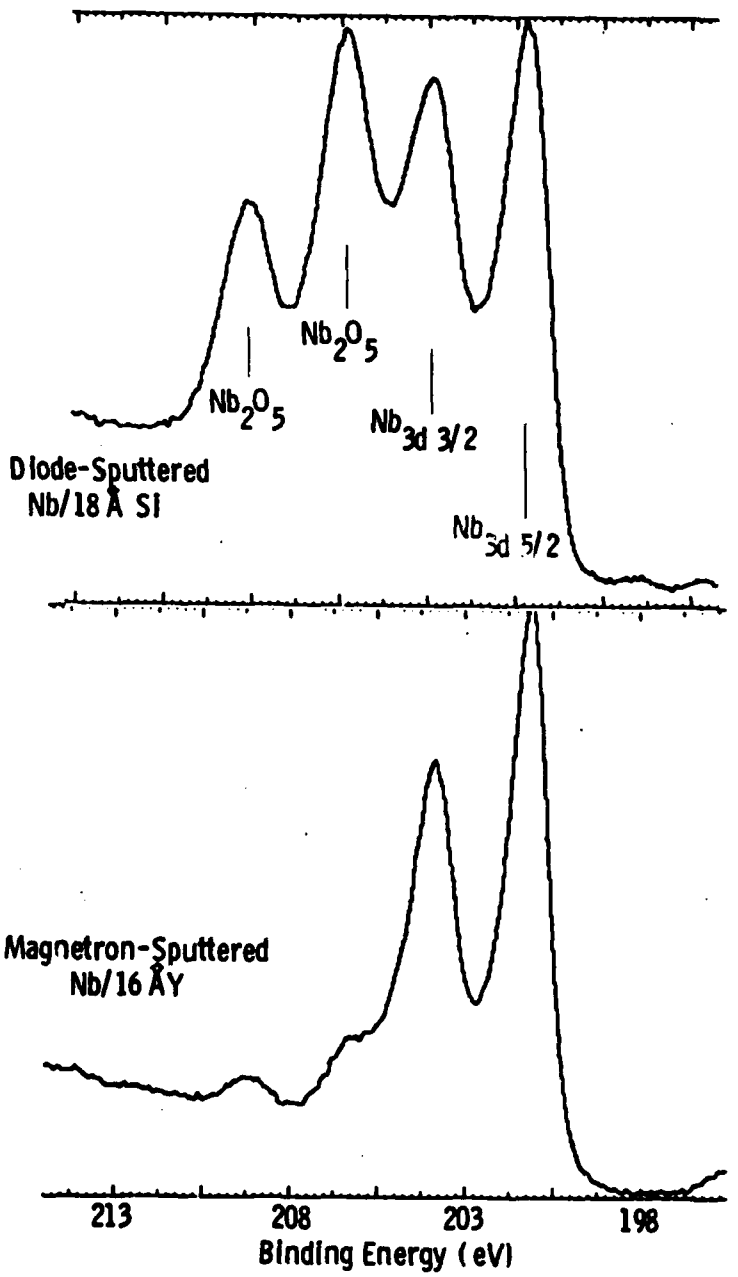

Figure 3.9 Niobium oxide growth from dc diode and dc magnetron sputtering.

Despite the dramatic difference between barrier properties of Nb/Y and Nb/Si bilayers illustrated in Figure 3.9, the dc tunneling characteristics were very similar. At 4.2 K, $\Delta_1 + \Delta_2 \approx 2.5$ meV for both types of junctions. The subgap leakage current was similarly high. Unlike other barriers, however, the Si was not completely oxidized while the base electrode had 25 Å of Nb_2O_5. Hence, an incomplete coverage by the Si was highly probable. The high leakage current through the exposed niobium oxide is not surprising in light of Halbritter's theory.[22]

The dc diode sputtered V_3Si/Si presented a contrast to Nb/Si. The V_3Si appeared to be protected by SiO_x barriers that were 23 Å and 31 Å thick according to XPS. Less than 1 Å of V_2O_5 could be seen by XPS at the normal observation angle (θ=0) as shown in Table 3.3. Note, however, that the nominal thickness of Si overlayers was 40 Å and 55 Å.

V_3Si samples prepared by reactive sputtering with a 42 Å thick Si barrier formed by the thermal decomposition of silane also had less than 1 Å of V_2O_5 at the base electrode/barrier interface. However, the XPS spectra recorded at a glancing angle (θ=80°) showed a difference in the base electrode oxidation that was not detectable at θ=0°. The glancing angle XPS spectra for $V_{2p3/2}$ photoelectrons are shown in Figure 3.10 for a diode sputtered bilayer of V_3Si/Si and a sample prepared by reactive sputtering and silane decomposition. Although both samples have a barrier which is nominally 40-42 Å thick, the diode sputtered barriers were measured by XPS to be only 23 Å. The silane decomposition sample appears to have no V_2O_5 but the diode sputtered bilayer has some V_2O_5 that was not detected at θ=0°. The difference either establishes the critical average barrier thickness needed to protect the V_3Si from oxidation to be between 23 and 40 Å or is due to a more uniform barrier coverage from silane decomposition. The two possibilities need to be tested by analyzing an available 25 Å Si overlayer deposited by SiH_4 decomposition. Insufficient data exists at present to determine whether the hydrogen which is present in the vacuum chamber during silane decomposition affects the barrier properties.

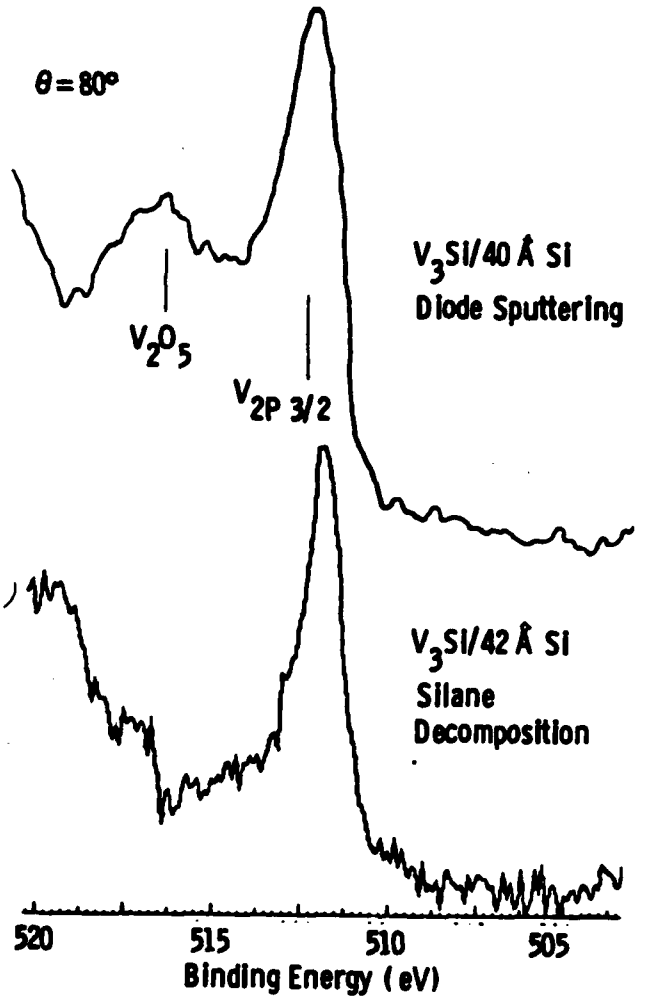

Figure 3.10 Vanadium oxidation measured at a glancing angle (θ=80°) for barriers formed by diode sputtering and by thermal decomposition of silane.

All V_3Si/SiOx/Pb junctions were shorts independent of the method of barrier formation.

In the case of junctions with sputtered overlayers the cause of shorts is not clear, while for those formed using SiH_4 decomposition shorts may be related to the sample geometry.

The V_3Si films formed by reactive sputtering coated the entire 6 mm x 6 mm substrate. Junction areas were defined by photoresist and Pb counterelectrodes were deposited as described in Section 2.5. An effort was made to avoid puncturing the Pb contact pads and photoresist with the probe pressure contacts during tunneling measurements. However, since all junctions measured were shorts, it is possible that the contacts punctured the photoresist and touched the V_3Si film underneath. *New samples prepared by reactive diode sputtering will conform to the standard geometry of Figure 2.6 with a 1 mm strip along two edges of the substrate masked during deposition to obviate the puncture problem.*

4. CONCLUDING DISCUSSION

Few definitive conclusions can be drawn based on the results presented. More open questions than answers have been produced to date. The purpose of this section is to summarize the status and define the main issues to be addressed in the second and third year of performance under this program.

Superconducting Film Electrodes

The XPS results of Section 3.2 and latest data by Ihara et al[11] indicate that the near-surface degradation of V_3Si upon oxidation is greatly aggravated by atomic segregation. In retrospect, V_3Si was probably not a happy choice of an A15 base material compared e.g. to Nb_3Al.[11] This might prove to be of no consequence, however, if total protection against the oxidation of the base electrode is provided by the overlayer. The use of V_3Si as a counterelectrode will probably require depositing a very thin metallic proximity layer on top of the oxide in order to minimize chances for atomic segregation. Luckily, this is not inconsistent with the proposed epitaxial approach to the high-T_c counterelectrode formation. A different A15 material such as Nb_3Al or Nb_3AlGe should be evaluated if problems with the near-surface atomic segregation persist.

Another significant observation made is that the V_3Si oxidation rate and depth is affected by humidity. In the study to date this must have resulted in accentuated near surface degradation of V_3Si films insufficiently protected by an overlayer.

The low oxygen affinity of Mo-Re (Table 3.1) was a slight surprise since Mo oxidizes readily. The Mo-Re appears now even more attractive as a counterelectrode material, and might be also of interest as a base electrode, at least for comparative purposes.

More work on Mo-Re synthesis must be done to attain a higher T_c, up to 14-15K, and to verify the possibility of low, near room tem-

perature synthesis. Results of magnetron sputtering and coevaporation in the SF should be compared, especially from the point of view of the impurity (oxygen) content effect upon the crystallization temperature.

Artificial Barriers

In accord with the Work Statement the barrier study by XPS concentrated on yttrium overlayers with aluminum as the first runner up. The XPS results made it clear that the ready formation of yttrium hydroxide makes of Y an overlayer more difficult to control than Al and Si when oxidizing in air of uncontrolled humidity. Indications were obtained, in accord with BTL observations[10] that humidity affects both the rate of formation, and the ultimate thickness of the oxide/hydroxide layer for both Y and Al. However, the effect is much more pronounced for yttrium. In the future the oxidation process should be performed *in situ* using dry oxygen or, when appropriate, a defined $O_2 + H_2O$ vapor mixture. This will be a natural solution once the S-I-S trilayer *in situ* fabrication is implemented.

The relative ability of the overlayer to protect the base underlayer against oxidation cannot yet be compared for Y, Al and Si since all Y layers, and all but one Al layers were oxidized throughout due to insufficient thickness and excessive oxidation time in humid air. These conditions also made it impossible to compare the results with those of BTL obtained for the Nb-base with various overlayers oxidized in low humidity air or dry oxygen, and deposited with table rotation.

The additional complicating factor is that the possibility of nonuniform overlayer coverage by any of the investigated elements deposited without rotation has not been excluded to date.

An estimate for Nb and V underlayer wetting based on Miedema's theory[20] predicts the wetting ability to decrease in the sequence Si, Al, Y. Results of Table 3.3 are consistent with that prediction.

At this juncture it is not yet possible to identify the most promising barrier material especially since the problem of interaction with high-T_c counterelectrodes has not yet been addressed. The relative

merits and demerits of alternative deposition processes *i.e.* magnetron sputtering vs pyrolysis vs evaporation are also still to be identified. A sufficient background of experience and reliable analytical data have been already accumulated to permit one the continuation of a comparative barrier study in conjunction with the second major object of this investgation: that of the high-T_c counterelectrode.

Tunnel Junctions

The cause(s) of the very high subgap leakage current observed in all measured Nb and V_3Si-base tunnel junctions free of shorts has (have) not yet been identified with 100% assurance. The common feature of all these junctions was, however, the insufficient protection against oxidation of the base electrode resulting in the formation of native oxides and, presumably, suboxides as well as in the atomic near-surface segregation in the case of V_3Si electrodes.

The depth of the superconductor degradation is not known, except that the XPS-determined native oxide thickness is below or much below the degradation depth. It is easy to rationalize the high leakage and a possible decrease in the gap voltage (Figures 3.4, 3.8 and their discussions) for V_3Si since the degradation depth is likely to be comparable to $\xi_{GL}(0)$ = 30 to 50 Å. For the Nb-base electrode, however, degradation should extend to a small fraction of $\xi_{GL}(0)$ ≈ 300 Å so that no gap decrease is to be expected, and the leakage must be related to the effective barrier (artificial plus native oxide) properties.

The one junction property that so far has not been used for diagnostic purposes is the product of normal resistance above the gap, R_n, and the junction area, A. It is typically orders of magnitude lower for the native oxides of comparable thickness than for high potential artificial barriers such as Y and Al. Hence, $R_n \cdot A$ can indicate whether the base coverage is complete and where the leakage originates. The analysis on $R_n \cdot A$ data is now in progress.

It is believed that once the full protection of the base is attained, low leakage current junctions will be fabricated without difficulty. The detailed steps to be taken (thicker overlayers, short oxidation time, humidity control, etc.) have been discussed in Section 3, and their implementation has the highest priority at this juncture.

Once low leakage tunneling characteristics are attained with a soft (Pb) counterelectrode the emphasis will shift to the study of refractory and high-T_c counterelectrodes, beginning with Nb and continuing into Mo-Re and V_3Si or another A15 probably identical with the base electrode. The refractory counterelectrode junctions will be patterned by reactive plasma etching from *in situ* fabricated trilayers. Both magnetron sputtering and e-beam evaporation will be used in a comparative mode that the integrated SF system will soon make practical. At that stage the I-V characteristics for both the superconducting and quasi-particle tunneling will be routinely determined, the control of critical current, I_c, will be addressed, and the specific capacitance of alternative barriers measured and compared.

5. ACKNOWLEDGMENTS

The authors acknowledge with gratitude the contribution of Mrs. B. P. Toth and Mrs. M. B. Cross who carefully typed this manuscript. We also thank Dr. M. Gurvitch of Bell Laboratories for friendly advice and suggestions.

6. REFERENCES

1. L. J. van der Pauw, "A Method of Measuring Resistivity and Hall Effect on Disks of Arbitrary Shape," Phil Res. Reports, 13:1 (1958).

2. M.Grundner and J. Halbritter, "XPS and AES Studies on Oxide Coatings on Niobium," J. Appl. Phys. 5(11): 397 (1980).

3. J. Kwo, G. W. Wertheim, M. Gurvitch, and D.N.E. Buchanan, "X-ray Photoemission Spectroscopy Study of Surface Oxidation of Nb/Al Overlayer Structures," Appl. Phys. Lett. 40(8): 675 (1982).

4. D. A. Rudman and M. R. Beasley, "Oxidized Amorphorus-Silicon Tunnel Junction Barriers," Appl. Phys. Lett., 36 (12): 1010 (1980).

5. Y. Tarutani, K. Yamada and U. Kawabe, "Superconducting Tunneling Junctions of V_3Si-SiO_x-Mo_3Re_2," Appl. Phys. Let., 37 (2): 239 (1980).

6. C. P. Umbach, A. M. Goldman and L. E. Toth, "Rare-Earth Oxides as Artificial Barriers in Superconducting Tunneling Junctions," Appl. Phys. Lett., 40(1): 81 (1982).

7. J. Kwo, G. K. Wertheim, M. Gurvitch, and D.N.E. Huchanan, "XPS and Tunneling Study of Air-Oxidized Overlayer Structures of Nb with Thin Mg, Y, and Er," IEEE Trans. on Magnetics MAG-19(3): 795 (1983).

8. M. Ronay E. E. Latta, "Interaction of Niobium Counterelectrodes with Yttrium Oxide Tunnel Barriers," Phys. Rev. B, 27: 1605 (1983).

9. H. Kroger, L. N. Smith and D. W. Jillie, "Selective Niobium Anodization Process for Fabricating Josephson Tunnel Junctions," Appl. Phys. Lett., 39 (3): 280 (1981).

10. M. Gurvitch, M. A. Washington, and H. A. Huggins, "High Quality Refractory Josephson Tunnel Junctions Utilizing Thin Aluminum Layers," Appl. Phys. Lett. 42 (5): 472 (1983) - also private communications.

11. H. Ihara, Y. Kimura, H. Okumura, K. Senzaki, and S. Gonda, "Oxidation Mechanism of the Surface of A15 Superconductors," Presented at the 1983 ICMC.

12. W. M. Riggs and M. J. Parker in Methods of Surface Analysis, edited by A. W. Czanderna, Elsevier, Amsterdam (1975).

13. V. Lacquaniti and R. Vaglio, "Properties of Niobium-Based Josephson Tunnel Junctions with a Lead-Indium Alloy Top Electrode," Cryogenics 22 (4): 188 (1982).

14. H.A.C.M. Bruning, "Homogeneity Regions and Superconducting Transition Temperatures in the System V-V_3Si," Phil. Res. Reports 22: 349 (1967).

15. A. S. Manocha, unpublished result.

16. J. R. Gavaler, M. A. Janocko, and C. K. Jones, "Superconductivity and Metastability in Alloys of the Mo-Re System," from Low Temperature Physics LT-13 Vol. 3, Plenum, N.Y. (1972).

17. R. D. Blaugher, A. Taylor, and J. K. Hulm, "The Superconductivity of Some Intermetallic Compounds," IMB J. of R. and D. 6 (1): 116 (1962).

18. M. M. Collver and R. H. Hammond, "Stability of Amorphous Transition-Metal Films," J. Appl. Phys., 49: 2420 (1978).

19. D. A. Rudman, "A15 Niobium-Tin: Fabrication and Superconductive Tunneling Spectroscopy," Ph.D. Thesis, Stanford University (1982).

20. A. R. Miedema and F. J. A. den Broede, "On the Interfacial Energy in Solid-Liquid and Solid-Solid Metal Combinations," Z. Metallkunde 70: 14 (1979) and references contained therein.

21. M. Grundner, "Surface Analysis of Nb for Superconducting Resonators Using XPS and AES " (in German), Kernforschungszentrum Report 2565 (Karlsruhe, 1977).

22. J. Halbritter, "On Resonant Tunneling in Nb-Nb_2O_5 Diodes," IEEE Trans. on Magnetics Mag-19 (3): 799 (1983).

23. G. E. Mullenberg (editor), Handbook of X-ray Photoelectron Spectroscopy, Perkin-Elmer Corp., Eden Prairie, Minn. (1979).

24. A. C. Gossard, F. J. DiSalvo, L. C. Erich, J. P. Remeika, H. Yasuoka, K. Kosuge, and S. Kachi, "Microscopic magnetic properties of vanadium oxides II. V_3O_5, V_5O_9, V_6O_{11}, and V_6O_{13}," Phys. Rev. B, 10(10); 4178 (1974).

25. C. C. Chang and D. M. Boulin, "Oxide Thickness Measurements up to 120 Å on Silicon and Aluminum Using the Chemically Shifted Auger Spectra," Surface Science 69: 385 (1977).

26. C. C. Chang, D. B. Fraser, M. J. Grieco, T. T. Sheng, S. E. Haszko, R. E. Kerwin, R. B. Marcus, and A. K. Sinha, "Aluminum Oxidation in Water," J. El. Chem. Soc., 125: 787 (1978).

7. ADDENDUM (11/20/83)

The experiment anticipated on page 49 of the Annual Report involving aluminum barriers which are not completely oxidized has been performed and has resulted in a marked improvement in junction properties. Tunnel junctions have been made on two sets of Nb/Al bilayers which were exposed to air for only 20 minutes. The first set of samples had 19 Å of Al_2O_3 on top of 8 Å of unoxidized Al as determined by XPS analysis. No niobium oxides were found when the detection angle was $\theta=0°$. At $\theta=80°$, however, a layer of Nb_2O_5 was found. The time between the end of the Nb deposition and the start of the aluminum deposition had been 11 minutes.

The second group of samples had 14 Å of Al_2O_3 on top of 2 Å of unoxidized Al (XPS data). The delay between the deposition of the two layers was only 2 minutes. There was no evidence of oxidation of the Nb base electrode in the XPS data collected at either $\theta=0°$ or 80°. Therefore, of the several possible causes of base electrode oxidation discussed on pages 37-41, the delay time between base electrode and barrier formation is most critical. *A method of cooling the substrates quickly has been devised and will have to be used with A-15 base electrodes which require a high substrate temperature during deposition.*

The I-V curve measured at 4.2 K for one of the latter group of samples is shown in Figure 7.1. A PbBi alloy with $T_c \simeq 8.4K$ and $\Delta \simeq 1.6$ meV was used in place of Pb as a counterelectrode and will be used until the trilayers are entirely deposited *in situ*. The niobium gap was therefore also $\Delta \simeq 1.6$ meV corresponding to the presence of high-T_c material ($\sim$9.2K) within a coherence length of the surface. Another indication of the quality of the surface layer was the low conductance below the gap characterized by I (4 mV)/I (2 mV) = 56.

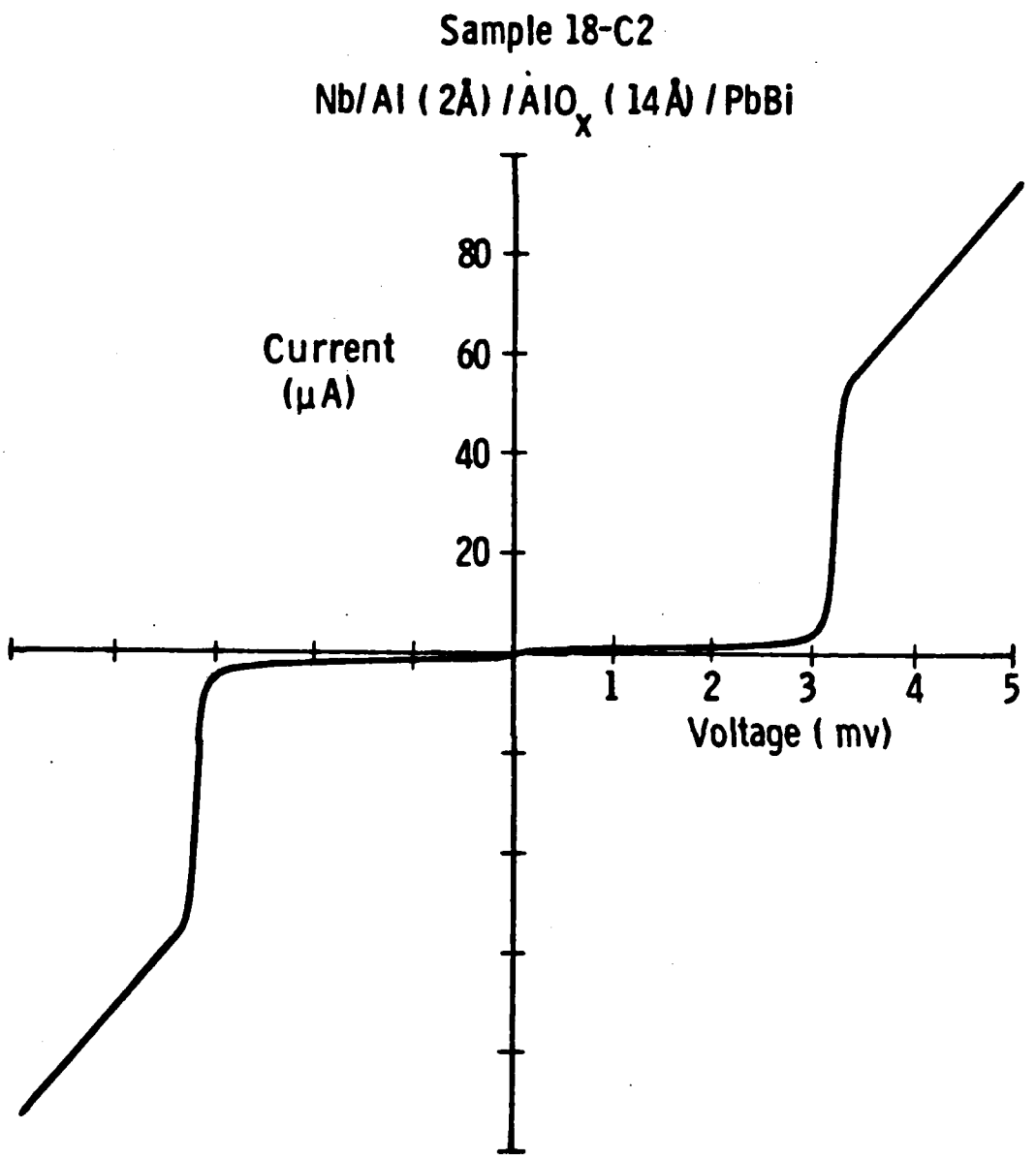

Figure 7.1 The dc tunneling characteristics of a Nb/Al/AlO$_x$/PbBi junction measured at 4.2K.

All of the other junctions from the two sets of Nb/Al bilayers as well as the one in Figure 7.1 show some leakage at zero voltage. Therefore, the barrier uniformity is still not ideal. Some improvement in coverage uniformity is to be expected if the sample holder is rotated during the barrier deposition (p. 56). The configuration of the magnetron sputtering chamber allows a one-dimensional oscillation of the substrates. *Barriers will be deposited with this oscillation for comparison with the static-substrate results.* An improvement in barrier uniformity should have the greatest effect on samples such as the one shown in Figure 7.1 which have only 2 Å of unoxidized aluminum protecting the base electrode from oxidation.

A lack of uniformity in the barrier was also evident in the junction resistances above the gap. The thicker barrier samples had higher resistances but the highest junction resistance on a single substrate was up to 2 times greater than the lowest resistance. The variation in resistance from one chip to another was as large as a factor of five. The conductance below the gap also varied from one junction to the next although I (4 mV)/I (2 mV) was generally greater than 10 for the samples with thin barrier and no Nb oxide and less than 10 for the thick barrier samples. For the junctions described in the report with completely oxidized barriers, I (4 mV)/I (2 mV) was always less than 3.

Suitable junction properties have been obtained to justify further routine characterization. *Primarily this means that I-V curves will be measured in a shielded dewar to obtain the dc Josephson current and dc measurements will be extended to high biases to extract the barrier energy height and width. The effect of short barrier oxidation times will be evaluated for V_3Si base electrodes with Al and V barriers.*

END

FILMED

2-84

DTIC